Electronic Supplementary Information (ESI)

Solid-state photoreactivity of 9-substituted acridizinium bromide salts

Samuel A. Stratford,[a] Mihails Arhangelskis,[a] Dejan-Krešimir Bučar*[ab] and William Jones*[a]

[a] Department of Chemistry, University of Cambridge, Lensfield Road, Cambridge CB2 1EW, United Kingdom
[b] Department of Chemistry, Department of Chemistry, University College London, 20 Gordon Street, London WC1H 0AJ, United Kingdom.

Table of content

1. Materials

4-Bromobenzyl bromide (98%), 4-iodobenzyl bromide (95%); 2-pyridine-carboxaldehyde (99%), benzene (≥99%), ethylene glycol (99+%), ethanol (absolute, ≥99.8%), sodium carbonate (ACS reagent, ≥99.5%) and DMSO-d_6, (99.9 atom % D) were obtained from *Sigma Aldrich*. 4-Chlorobenzyl bromide (98+%), 4-fluorobenzyl bromide (97%), 4-methylbenzyl bromide (98%), 4-*tert*-butylbenzyl bromide (97%), *p*-toluenesulfonic acid monohydrate (97%), hydrobromic acid (48% *w/w* aq. soln.) were obtained from *Alfa-Aesar*. Acetonitrile (99.99%) and sodium sulfate (anhydrous, ≥99.0%) were purchased from *Fisher*. Sulfolane (≥99%) was obtained from *Merck*. All reagents and solvents were used as received.

2. Synthesis and ^{1}H NMR characterisation

2.1. Synthesis of 2-(1,3-dioxolan-2-yl)pyridine

2-(1,3-Dioxolan-2-yl)pyridine was synthesised following the procedure of Hobson *et al.*[1] A suspension composed of 21.4 g (200 mmol) of 2-pyridinecarboxaldehyde, 10 g (58 mmol) of *p*-toluenesulfonic acid, 25 mL (450 mmol) of ethylene glycol and 300 mL of benzene was stirred and refluxed in the dark for three days. The resulting solution was extracted with an aqueous solution of sodium carbonate. The obtained aqueous layer was subsequently washed with three fractions of benzene. The obtained benzene solutions were dried with sodium sulfate, combined and evaporated under reduced pressure to obtain a viscous brown liquid. The product was distilled under reduced pressure (1.1 kPa) to obtain a light yellow viscous liquid. Yield: 58-61%. ^{1}H NMR (δ ppm): 8.53 (ddd, $J = 4.9$, 1.8, 1.0 Hz, 1H), 7.81 (td, $J = 7.7$, 1.8 Hz, 1H), 7.50 (dt, $J = 7.9$, 1.1 Hz, 1H), 7.36 (ddd, $J = 7.6$, 4.8, 1.2 Hz, 1H), 5.71 (s, 1H), 4.13 − 3.84 (m, 4H) (Figure S1).
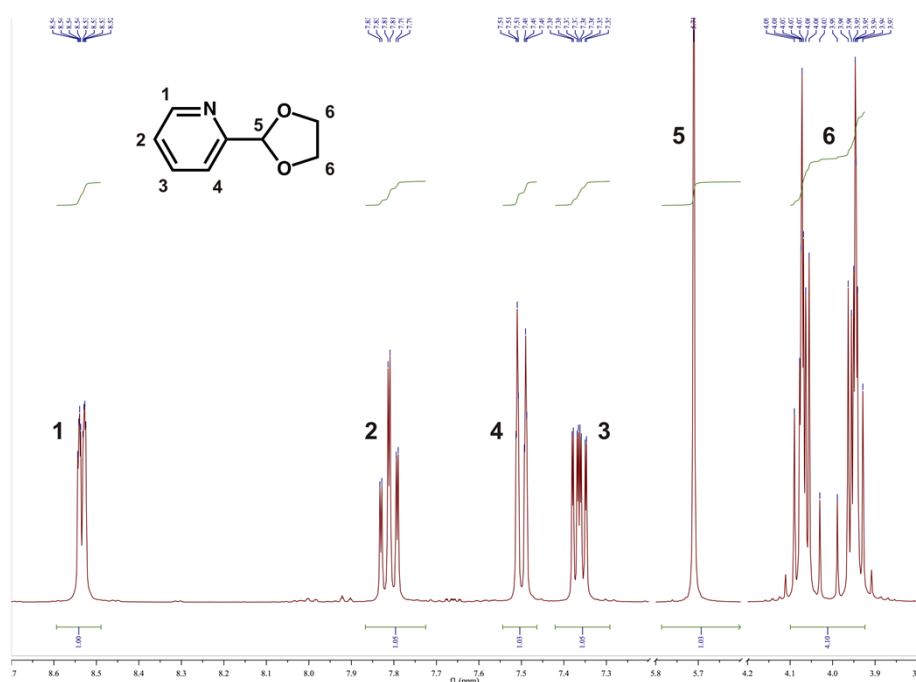

Figure S1. ^{1}H NMR spectrum of the pyridine precursor 2-(1,3-dioxolan-2-yl)pyridine.

2.2. Synthesis of 1-(4-X-benzyl)-2-(1,3-dioxolan-2-yl)pyridin-1-ium bromide (where X = F, Cl, Br, I, CH₃, C(CH₃)₃) (3-X)

The compound was prepared according to procedures published by Bradsher *et al.*[2,3] In a typical experiment, a total of 10 mmol of a 4-X-benzyl bromide was added to a solution of 2-(1,3-dioxolan-2-yl)pyridine (1.59 g, 10 mmol) in tetramethylene sulfone (sulfolane) (4 ml). The obtained suspension was stirred in a sealed flask for 4 days at room temperature. The resulting oily substance was triturated with ethyl acetate to obtain a crude solid of 1-(4-X-benzyl)-2-(1,3-dioxolan-2-yl)pyridin-1-ium bromide (3-X). Yields: 3.30 g, 97% (3-F); 3.17 g, 89% (3-Cl); 3.70 g, 93% (3-Br); 4.45 g, 99% (3-I-Br); 3.08 g, 91% (3-CH₃); 3.16 g, 84% (3-C(CH₃)₃). Results of ^{1}H NMR analyses:

1) **3-F** ^{1}H NMR ($\square$ ppm): 9.00 (dd, J = 6.1, 1.3 Hz, 1H), 8.70 (td, J = 7.8, 1.3 Hz, 1H), 8.31 (dd, *J* = 8.0, 1.5 Hz, 1H), 8.18 (ddd, *J* = 7.7, 6.1, 1.7 Hz, 1H), 7.52 – 7.40 (m, 2H), 7.29 (t, *J* = 8.8 Hz, 2H), 6.53 (s, 1H), 5.97 (s, 2H), 4.12 (s, 4H).

2) **3-Cl** ^{1}H NMR ($\square$ ppm): 9.04 (dd, *J* = 6.2, 1.4 Hz, 1H), 8.72 (td, *J* = 7.9, 1.4 Hz, 1H), 8.31 (dd, *J* = 8.0, 1.6 Hz, 1H), 8.20 (ddd, *J* = 7.8, 6.2, 1.6 Hz, 1H), 7.51 (d, *J* = 8.5 Hz, 2H), 7.39 (d, *J* = 8.5 Hz, 2H), 6.52 (s, 1H), 5.99 (s, 2H), 4.10 (s, 4H).

3) **3-Br** ^{1}H NMR ($\square$ ppm): 9.03 (dd, *J* = 6.2, 1.3 Hz, 1H), 8.72 (td, *J* = 7.9, 1.4 Hz, 1H), 8.31 (dd, *J* = 8.1, 1.6 Hz, 1H), 8.19 (ddd, *J* = 7.8, 6.1, 1.6 Hz, 1H), 7.64 (d, *J* = 8.5 Hz, 2H), 7.31 (d, *J* = 8.5 Hz, 2H), 6.50 (s, 1H), 5.97 (s, 2H), 4.10 (s, 4H).

4) **3-I-Br** ^{1}H NMR ($\square$ $\square$ppm): 9.01 (dd, *J* = 6.2, 1.3 Hz, 1H), 8.71 (td, *J* = 7.9, 1.4 Hz, 1H), 8.31 (dd, *J* = 8.1, 1.6 Hz, 1H), 8.18 (ddd, *J* = 7.8, 6.1, 1.6 Hz, 1H), 7.80 (d, *J* = 8.4 Hz, 2H), 7.14 (d, *J* = 8.4 Hz, 2H), 6.49 (s, 1H), 5.94 (s, 2H), 4.10 (s, 4H)

5) **3-CH$_3$** ^{1}H NMR ($\square$ ppm): 8.99 (dd, *J* = 6.2, 1.4 Hz, 1H), 8.69 (td, *J* = 7.9, 1.4 Hz, 1H), 8.30 (dd, *J* = 8.1, 1.6 Hz, 1H), 8.17 (ddd, *J* = 7.8, 6.2, 1.6 Hz, 1H), 7.25 (s, 4H), 6.50 (s, 1H), 5.93 (s, 2H), 4.12 (s, 4H), 2.30 (s, 3H)

6) **3-C(CH$_3$)$_3$** ^{1}H NMR ($\square$ $\square$ppm): 9.00 (dd, *J* = 6.2, 1.4 Hz, 1H), 8.70 (td, *J* = 7.9, 1.4 Hz, 1H), 8.31 (dd, *J* = 8.0, 1.6 Hz, 1H), 8.18 (ddd, *J* = 7.8, 6.2, 1.6 Hz, 1H), 7.45 (d, *J* = 8.4 Hz, 2H), 7.28 (d, *J* = 8.4 Hz, 2H), 6.51 (s, 1H), 5.93 (s, 2H), 4.13 (s, 4H), 1.26 (s, 9H)

All ^{1}H NMR spectra were recorded using a *Bruker Avance III 400 QNP Ultrashield Plus Cryo* spectrometer operating at 400 MHz, while the ^{13}C NMR spectra were acquired at 100 MHz. All spectra were obtained using DMSO-d_6 as solvent. The spectra were analysed using the *MestReNova* software package (*v*.7.1.1-9649). The ^{1}H NMR spectra of **3-X** are shown in Figure S2-S7.
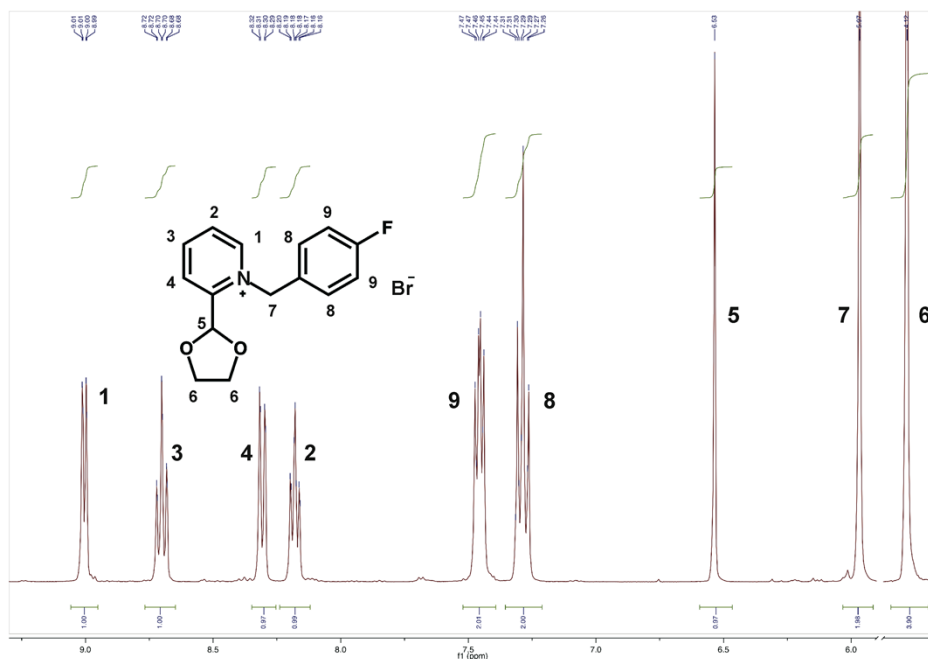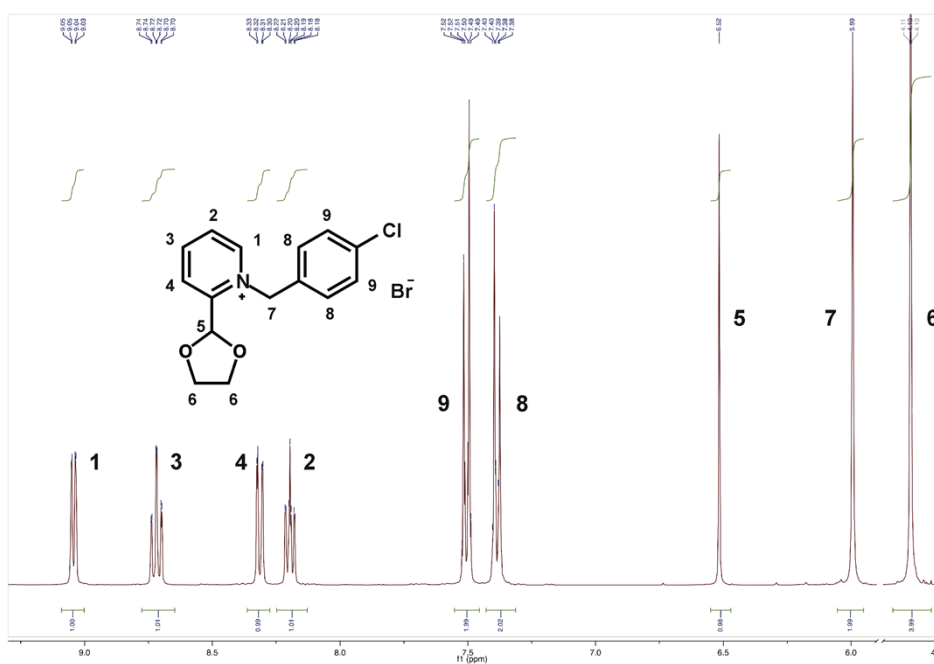
Figure S2. ^{1}H NMR spectrum of **3-F**.

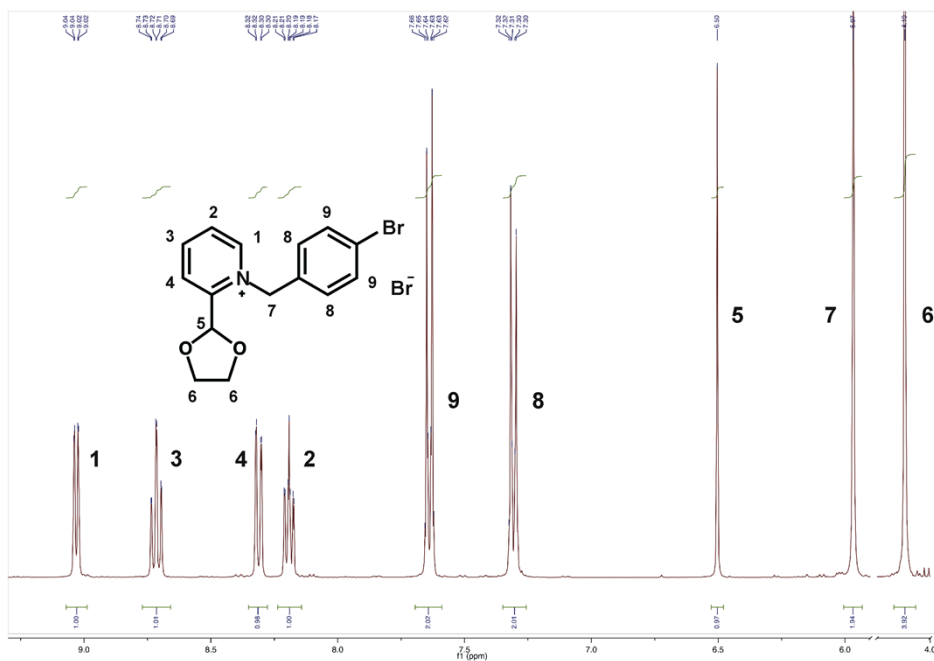**Figure S3.** ^{1}H NMR spectrum of **3-Cl**.

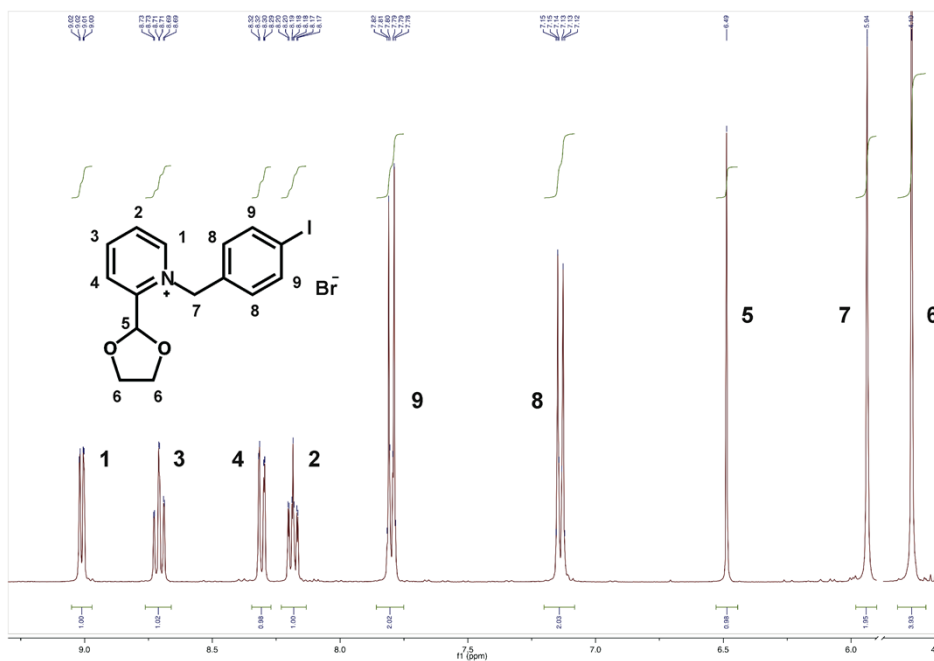**Figure S4.** ^{1}H NMR spectrum of **3-Br**.

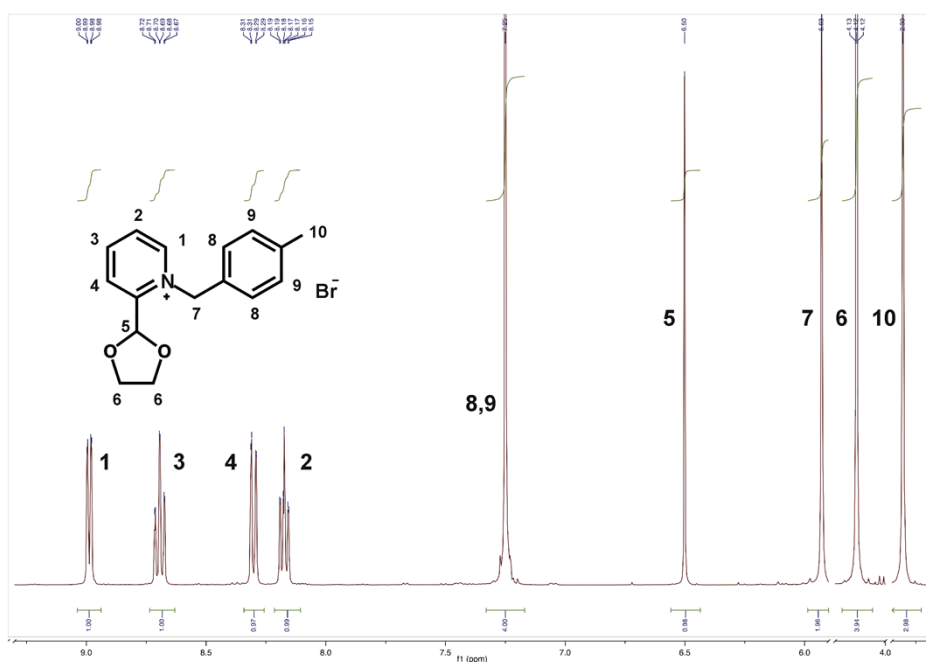**Figure S5.** ^{1}H NMR spectrum of **3-I**.

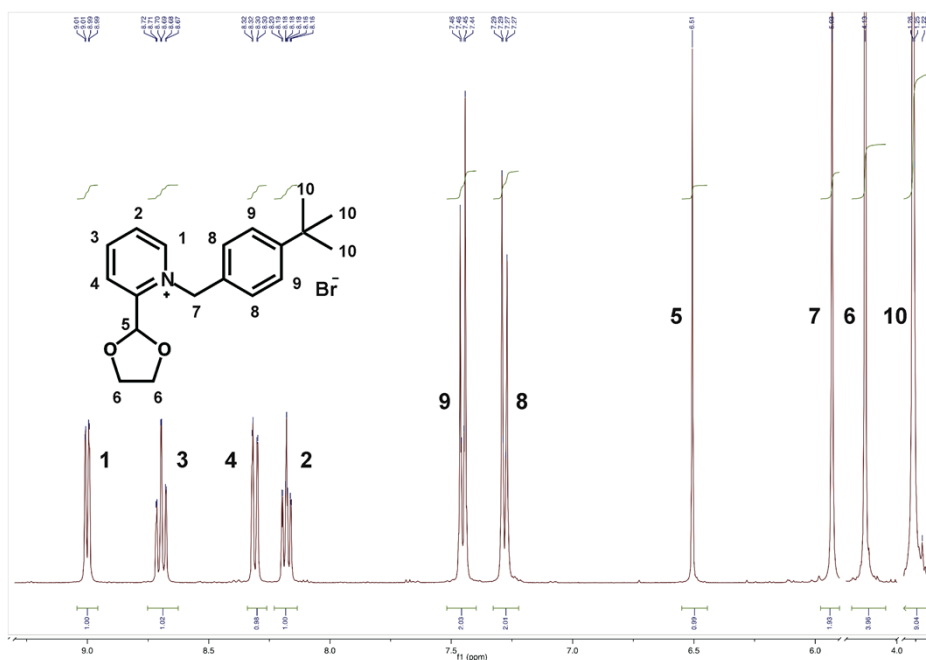**Figure S6.** ^{1}H NMR spectrum of **3-CH₃**.

Figure S7. ^{1}H NMR spectrum of **3-C(CH₃)₃**.

2.3. Cyclisation of 1-(4-X-benzyl)-2-(1,3-dioxolan-2-yl)pyridin-1-ium bromides to 9-substituted acridizinium bromide monohydrates (9-X)

A total of 5 mL of 48% hydrobromic acid in water was added to 5 mmol of **3-X**, and refluxed for 12 hours. The acid was then removed by rotary evaporation to yield the crude 9-X-acridizinium bromides (**9-X**). The **9-X** salts were purified by recrystallisation using ethanol as solvent. All salts were obtained phase pure, except **9-C(CH$_3$)$_3$** (see section 3.2). Yields: 0.61 g, 36% (**9-F**); 1.48 g, 83% (**9-Cl**); 1.38 g, 69% (**9-Br**); 1.50 g, 67% (**9-I-Br**); 1.06 g, 63% (**9-CH$_3$**); 1.65 g, 87% (**9-C(CH$_3$)$_3$**, mixture of two or more phases). The ^{1}H NMR spectra of **9-X** are shown in Figure S8-S13.

Results of ^{1}H NMR analyses:

1) **9-F** ^{1}H NMR (☐ ☐☐ppm): 10.47 (s, 1H), 9.25 (d, J = 7.0 Hz, 1H), 9.14 (s, 1H), 8.62 (dd, J = 9.4, 5.6 Hz, 1H), 8.54 (dd, J = 8.9, 1.2 Hz, 1H), 8.22 (dd, J = 9.7, 2.5 Hz, 1H), 8.07 (ddd, J = 8.7, 7.0, 1.1 Hz, 1H), 7.97 – 7.88 (m, 2H).
2) **9-Cl** ^{1}H NMR (☐ ☐☐ppm): 10.49 (s, 1H), 9.33 – 9.25 (d, 1H), 9.15 (s, 1H), 8.67 – 8.57 (d, 2H), 8.53 (d, 1H), 8.18 – 8.07 (t, 1H), 8.05 – 7.92 (m, 2H).
3) **9-Br** ^{1}H NMR (☐ ☐☐ppm): 10.47 (s, 1H), 9.33 - 9.25 (d, 1H), 9.14 (s, 1H), 8.76 (s, 1H), 8.65 - 8.56 (d, 1H), 8.43 (d, J = 9.2 Hz, 1H), 8.10 (m, 2H), 7.99 (t, 1H)
4) **9-I-Br** ^{1}H NMR (☐ ppm): 10.42 (s, 1H), 9.26 (d, J = 7.0 Hz, 1H), 9.09 (s, 1H), 8.95 (s, 1H), 8.58 (d, J = 8.9 Hz, 1H), 8.33 – 8.16 (m, 2H), 8.08 (t, J = 8.9, 6.9 Hz, 1H), 8.03 – 7.92 (t, 1H).
5) **9-CH$_3$** ^{1}H NMR (☐ ☐☐ppm): 10.37 (s, 1H), 9.22 (d, J = 7.3 Hz, 1H), 9.06 (s, 1H), 8.51 (d, J = 9.0 Hz, 1H), 8.38 (d, J = 8.7 Hz, 1H), 8.14 (s, 1H), 8.06 – 7.97 (t, 1H), 7.94 – 7.82 (m, 2H), 2.64 (d, J = 1.0 Hz, 3H).
6) **9-C(CH$_3$)$_3$** ^{1}H NMR (☐ ☐☐ppm): 10.37 (s, 1H), 9.24 (d, J = 7.0 Hz, 1H), 9.15 (s, 1H), 8.51 (d, J = 8.9 Hz, 1H), 8.42 (d, J = 9.1 Hz, 1H), 8.26 (s, 1H), 8.18 (d, J = 9.0, 1H), 8.03 (t, J = 8.9, 1H), 7.97 – 7.86 (t, 1H), 1.44 (s, 9H).
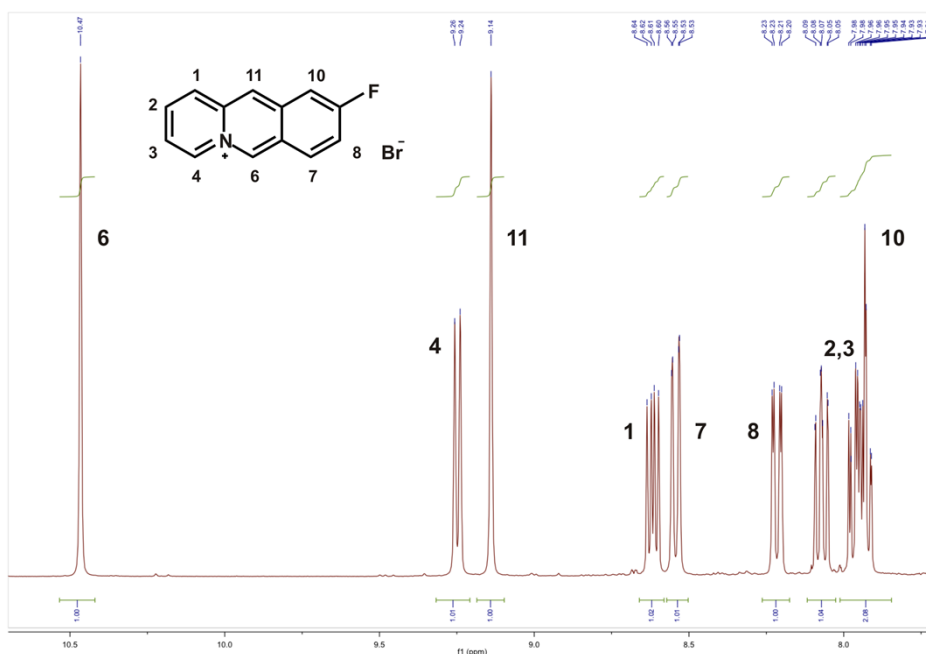

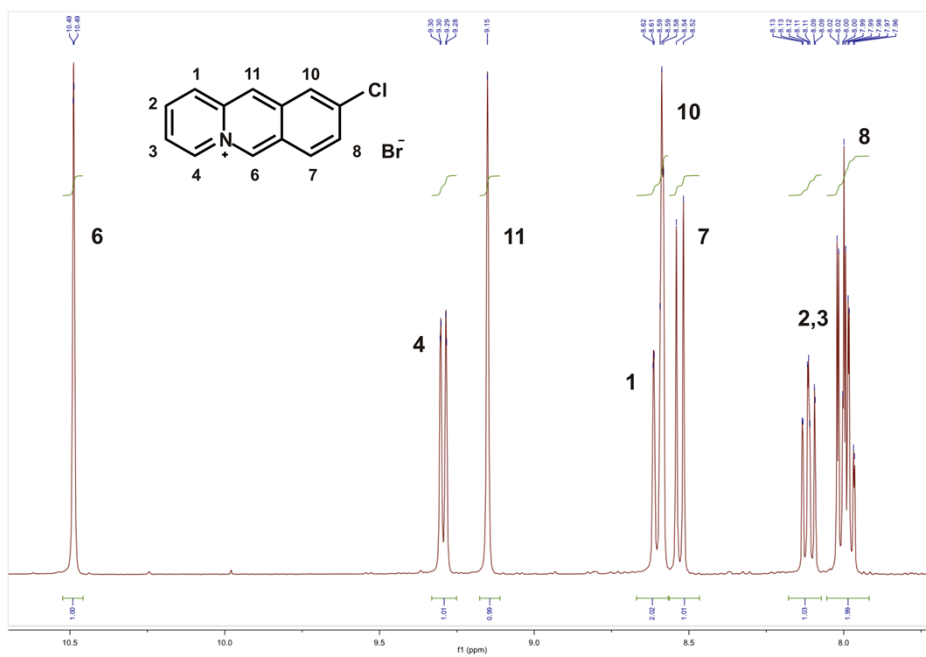**Figure S8.** ^{1}H NMR spectrum of **9-F**.
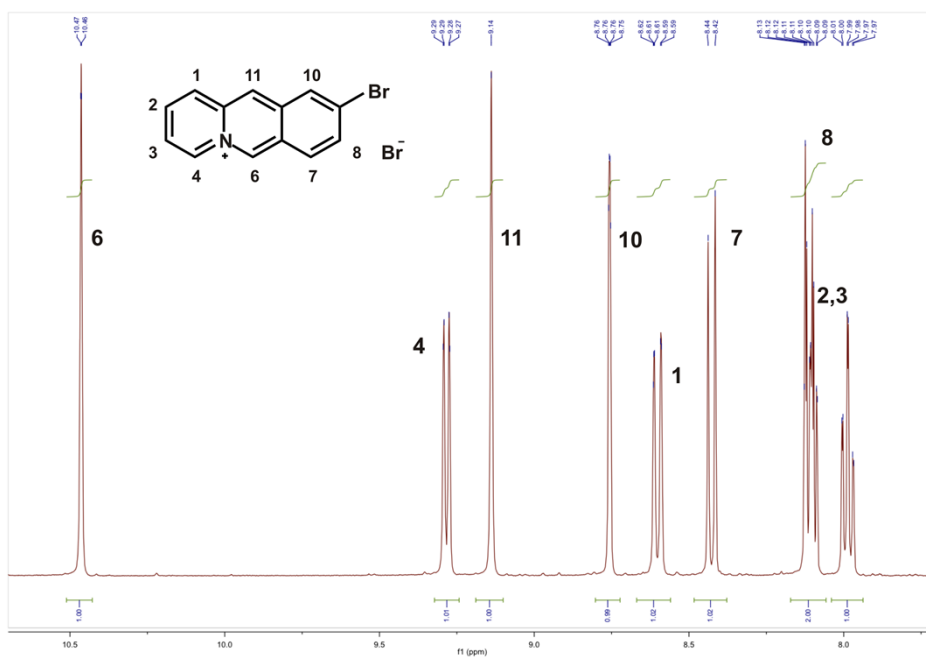
Figure S9. ^{1}H NMR spectrum of **9-Cl**.

Figure S10. ^{1}H NMR spectrum of **9-Br**.
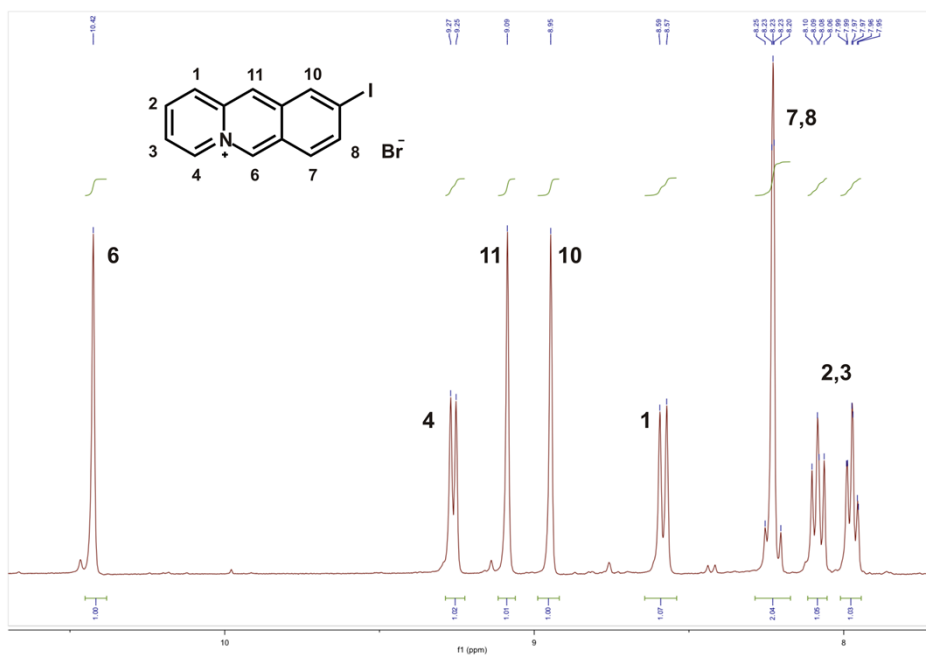
Figure S11. ^{1}H NMR spectrum of **9-I-Br**.
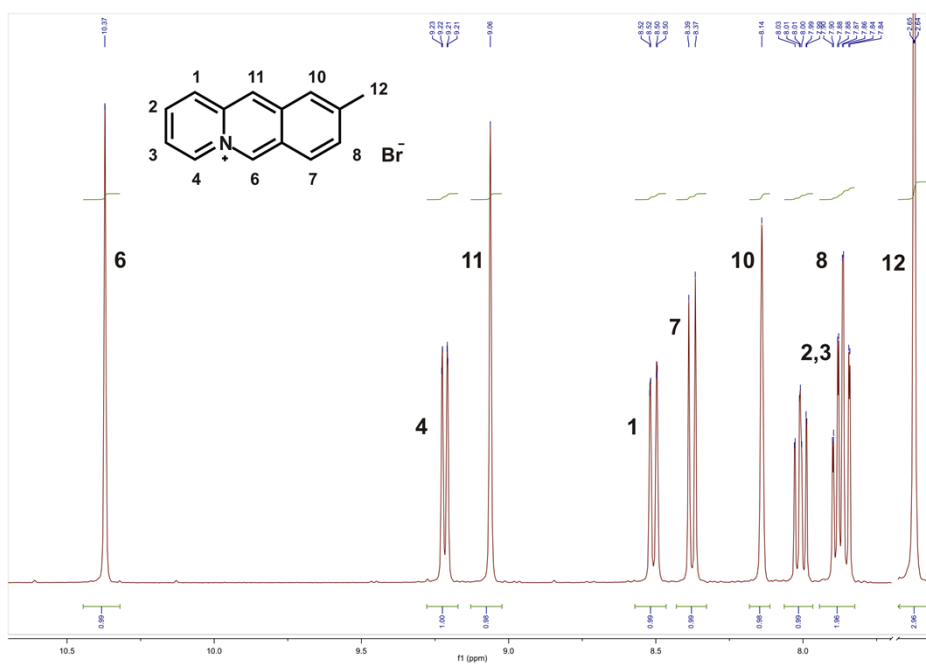
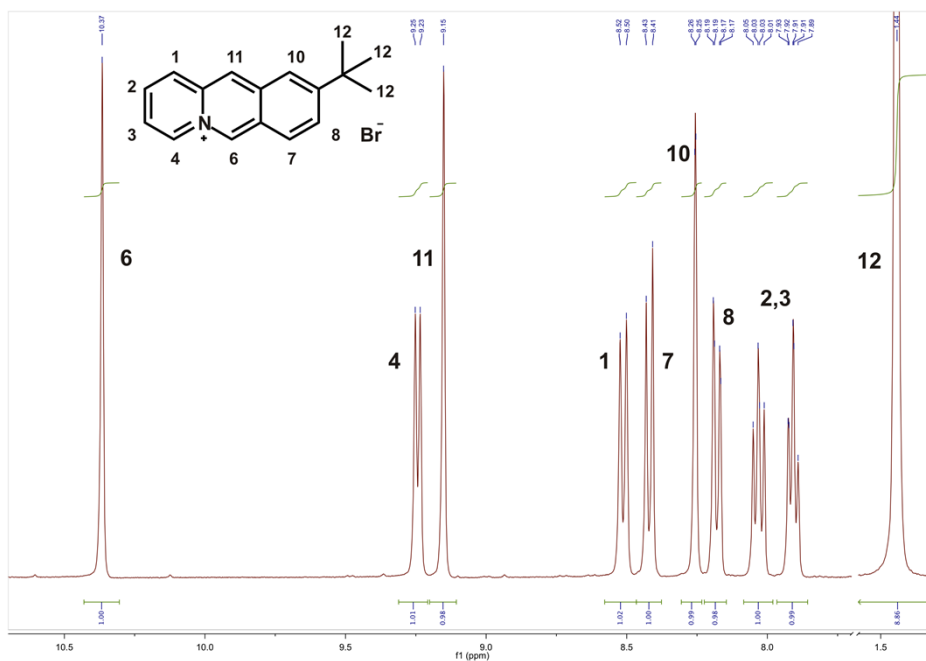**Figure S12.** ^{1}H NMR spectrum of **9-CH$_3$**.

Figure S13. ^{1}H NMR spectrum of **9-C(CH$_3$)$_3$**.

3. Crystallisation Experiments

3.1. Single crystal growth

In a typical crystallisation experiment, about 10 mg of a **9-X** were dissolved in 2-5 mL of hot EtOH. The obtained solution was filtered through a cotton plug and left to evaporate slowly in a partially covered crystallisation vial at ambient conditions. Crystals suitable for single crystal X-ray diffraction experiments were obtained in up to three days.

Attempts to grow single crystals of **9-C(CH$_3$)$_3$** from EtOH, MeOH, *i*-PrOH, *t*-BuOH, acetonitrile, chloroform, acetone, DMF and DMSO were unsuccessful. The crystal structure of **9-C(CH$_3$)$_3$** was therefore determined using PXRD data.

3.2. Crystallisation of 9-C(CH$_3$)$_3$

Whereas **9-F**, **9-Cl**, **9-Br**, **9-I** and **9-CH$_3$** were obtained phase pure by recrystallization of the synthesised bulk material, the recrystallization of **9-C(CH$_3$)$_3$** resulted in the formation of a mixture of **9-C(CH$_3$)$_3$** phases. To obtain a phase pure bulk of **9-C(CH$_3$)$_3$**, the solid was heated to 120 °C to dehydrate for one hour and subsequently left at ambient conditions to rehydrate overnight (the obtained solid is fairly hygroscopic). The PXRD traces of the as-synthesised, as well as the dehydrated and subsequently rehydrated **9-C(CH$_3$)$_3$** single phase are shown in Fig. S19.

4. Structural analyses

4.1. Single crystal X-ray diffraction studies of 9-F, 9-Cl, 9-Br, 9-I-Br, 9-I-I$_3$, 9-CH$_3$ and the 9-C(CH$_3$)$_3$ photodimer

All single crystals were investigated using a *Nonius KappaCCD* single crystal X-ray diffractometer using MoK_α radiation ($\lambda = 0.71073$ Å) generated at 50 kV and 30 mA. The diffraction datasets were collected and processed using *Collect*[4] and *HKL Scalepack/Denzo*[5] The diffraction images were collected in φ and ω scans. The structures were solved using direct methods (using SHELXS[6]) refined on F^2 by weighted full-matrix least-squares (using SHELXL[6]). All non-hydrogen atoms that were missed in the initially obtained model were subsequently identified from the difference Fourier map within several refinement steps. All non-hydrogen atoms were refined anisotropically. Hydrogen atoms associated with carbon atoms were refined in geometrically constrained positions with isotropic displacement parameters fixed at 1.2 times $U_{eq}(C)$. Hydrogen atoms of water molecules were (if possible) located in difference Fourier maps as small electron densities in the final stages of the refinement procedures. Their positions were refined with isotropic displacement parameters fixed at 1.5 times $U_{eq}(O)$ using restraints. The crystal structures of **9-F**, **9-Cl**, **9-Br**, **9-I-Br**, **9-I-I$_3$**, **9-CH$_3$** are described in the main text. The crystal structure of the **9-C(CH$_3$)$_3$** photodimer is described below. Crystallographic and refinement parameters for all single crystals X-ray structures are given in Table S1.

The data quality for the **9-I-Br**, **9-I-I$_3$** and the **9-C(CH$_3$)$_3$-photodimer** structures is relatively poor. The investigated single crystals were small in size and diffracted poorly despite the presence of heavy atoms.

Table S1. Crystallographic and refinement parameters for crystal structures solved from single crystal X-ray diffraction data.

Compound reference	9-F	9-Cl	9-Br	9-I-Br
Chemical formula	$C_{13}H_{11}BrFNO$	$C_{13}H_9BrClNO_{0.75}$	$C_{13}H_{11}Br_2NO$	$C_{13}H_{11}BrINO$
Formula Mass	296.14	308.07	357.05	404.01
Crystal system	monoclinic	triclinic	triclinic	monoclinic
a/Å	10.4896(4)	9.5818(3)	7.3152(6)	7.5841(6)
b/Å	12.9381(5)	11.4519(3)	9.7141(9)	19.2894(16)
c/Å	9.9423(3)	12.5667(4)	10.352(2)	9.3211(9)
α/°	90.00	109.027(2)	68.687(3)	90.00
β/°	117.876(3)	94.230(2)	86.209(3)	105.886(4)
γ/°	90.00	105.253(2)	68.298(4)	90.00
V/Å^3	1192.75(7)	1238.29(6)	634.75(15)	1311.5(2)
T/K	270(2)	298(2)	298(2)	298(2)
Space group	$P2_1/c$	P**Error!**	P**Error!**	$P2_1/c$
Z	4	4	2	4
μ/mm^{-1}	3.441	3.514	6.367	5.471
$F(000)$	592	614	348	768
reflections measured	9072	16387	4583	6457
independent reflections	2153	4355	2194	1676
R_{int}	0.0462	0.0482	0.0495	0.1114
R_1 values ($I > 2\sigma(I)$)	0.0391	0.0467	0.0799	0.0477
$wR(F^2)$ values ($I > 2\sigma(I)$)	0.0988	0.1107	0.2424	0.1057
R_1 values (all data)	0.0643	0.0660	0.1223	0.0716
$wR(F^2)$ values (all data)	0.1032	0.1208	0.2541	0.1170
Goodness of fit on F^2	1.062	1.046	1.039	1.075
CCDC reference number	975287	975288	975289	975290

Compound reference	9-I-I$_3$	9-CH$_3$	9-C(CH$_3$)$_3$-photodimer
Chemical formula	$C_{13}H_9I_4NO_0$	$C_{14}H_{14}BrNO$	$C_{34}H_{40}Br_2N_2O$
Formula Mass	686.81	292.17	650.48
Crystal system	triclinic	triclinic	triclinic
a/Å	7.5081(3)	7.7990(10)	7.7034(7)
b/Å	10.4940(5)	9.585(2)	9.1410(10)
c/Å	11.7322(6)	9.664(2)	12.257(2)
α/°	105.219(2)	68.967(7)	88.730(6)
β/°	105.581(2)	70.925(6)	78.321(6)
γ/°	101.791(2)	83.339(6)	71.486(4)
V/Å^3	820.76(7)	637.3(2)	800.65(17)
T/K	180(2)	298(2)	293(2)
Space group	P**Error!**	P**Error!**	P**Error!**
Z	2	2	1
μ/mm^{-1}	7.577	3.208	2.559
$F(000)$	612	296	334
reflections measured	9366	5002	4589
independent reflections	2862	2188	2055
R_{int}	0.0924	0.0712	0.0586
R_1 values ($I > 2\sigma(I)$)	0.1155	0.0611	0.0586
$wR(F^2)$ values ($I > 2\sigma(I)$)	0.3405	0.1552	0.1529
R_1 values (all data)	0.1399	0.0936	0.0779
$wR(F^2)$ values (all data)	0.3512	0.1689	0.1666
Goodness of fit on F^2	1.130	1.002	1.134
CCDC reference number	975291	975292	975293

4.1.1. Crectal structure of the *anti*-**ht** photodimer of **9-C(CH₃)₃**

The attempts to crystallise **9-C(CH₃)₃** from an EtOH solution yielded single crystals of the *anti*-**ht** photodimer of **9-C(CH₃)₃**, which formed in a closed crystallisation vial that was unintentionally left exposed to sunlight for about a week. A single crystal X-ray diffraction analysis revealed that the *anti*-**ht** photodimer (Fig. S14) crystallises in the triclinic *P***Error!** space group with one half of photodimer, one bromide anion and one water molecule in the asymmetric unit. The photodimers and bromide-water hydrate assemblies interact *via* C-H···Br and π···π interactions.
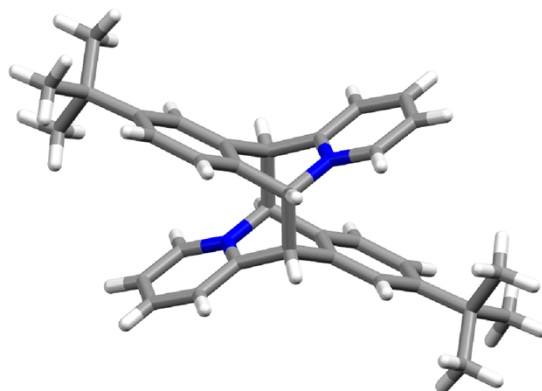
Figure S14. X-ray crystal structure of the *anti*-**ht** photodimer of the **9-C(CH₃)₃** cation.

4.2. Structure determination of 9-C(CH₃)₃ *via* powder X-ray diffraction and plane-wave DFT calculations

The powder X-ray diffraction data was collected at room temperature using a laboratory *Stoe StadiP* powder X-ray diffractometer using monochromated Cu$K_{\alpha 1}$ radiation ($\lambda = 1.5406$ Å) generated at 40 kV and 30 mA. The transition-geometry diffractometer was equipped with a *DECTRIS MYTHEN 1K* detector. The data collection was controlled using the *Stoe Win XPOW* program (v3.0.2.7). The powder sample was set in a 0.5 mm borosilicate capillary. The data collection was performed in the continuous mode in the 2θ range of 2.0-60.0° with a 0.5° step size and a counting time of 20 s/step.

The X-ray powder pattern of **9-C(CH₃)₃** was indexed by the program *DICVOL06*[8] with the aid of the interface of *DASH 3.2*.[9] Simulated annealing structure solution and Rietveld refinement[10] was performed using the *TOPAS Academic 4.1* program.[7] The peak shapes were described using a pseudo-Voigt function, the background was computed using Chebyshev polynomials and the 9-*tert*-butylacridizinium cation was treated as rigid body during the structure solution and refinement.

The resulting crystal structure was optimised using the plane-wave DFT code *CASTEP 6.1*.[11] The calculations were performed using the PBE exchange-correlation functional,[12] G06 dispersion correction[13] and norm-conserving pseudopotentials[14] with the plane wave cut-off set to 700 eV. The k-point spacing was set to 0.04 A⁻¹. The correctness of structure determination was verified by the close similarity of the experimental and DFT-optimised structures. The final Rietveld refinement was

performed using the molecular geometry of acridizinium moieties extracted from the DFT-optimised structures. The Rietveld plot is shown in Fig. S15. Crystallographic and refinement parameters for the powder X-ray structure of **9-C(CH₃)₃** are given in Table S2.
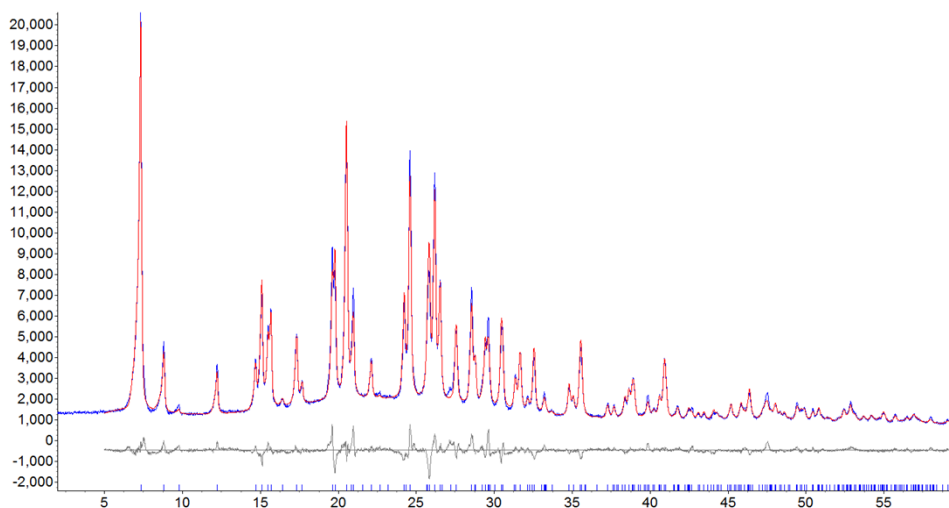

Figure S15. Rietveld plot for **9-C(CH₃)₃** (*red*: calculated, *blue*: measured, *grey*: difference). The peak positions are represented with tick marks (*x*-axis: 2θ values, *y*-axis: counts).

Table S2. Crystallographic and refinement parameters for **9-C(CH₃)₃** obtained from powder X-ray diffraction data.

Chemical formula	$C_{17}H_{20}BrNO$
M_r	334.26
Crystal system	orthorhombic
a/Å	18.08801(59)
b/Å	12.04679(49)
c/Å	7.22980(19)
α/°	90
β/°	90
γ/°	90
V/Å³	1575.39(9)
T/K	295
Space group	$Pca2_1$
Z	4
Radiation type	$CuK_{\alpha1}$
R_{wp}	0.054
R_{Bragg}	0.021
CCDC deposition number	992871

4.3. Qualitative powder X-ray diffraction (PXRD) studies of the 9-X salts

The powder X-ray diffraction data for **9-F**, **9-Br**, **9-I-Br**, **9-CH₃**, **9-C(CH₃)₃** was collected using the *Stoe StadiP* powder X-ray diffractometer described in section 4.2. The powder sample was placed in a 0.5 mm borosilicate capillary, while the data collection was performed in the continuous mode in the 2θ range of 2.0-60.0° with a 0.5° step size and a counting time of 25 s/step.

The powder-diffraction data for **9-Cl** was collected using a laboratory *Panalytical X'pert PRO* powder diffractometer (Bragg-Brentano geometry) using Ni-filtered CuK_α radiation ($\lambda = 1.5418$ Å) generated at 40 kV and 40 mA. The sample was placed into a flat glass sample holder. The scans were performed in the continuous mode (gonio scan axis) in the 2θ range of 0-60.0° (counting times of 40 s, step size of 0.0334°). The data was analysed using the *X'Pert HighScore Plus* v2.2 program.

Rietveld refinements of the obtained single crystal structures against the experimental PXRD patterns were performed to demonstrate that all prepared bulk materials are phase pure. The refinements were accomplished using the program *TOPAS Academic 4.1.*[7] The calculation for sample **9-Cl** suffered from moderate preferred orientation of the crystallites. The preferred orientation was caused by the non-uniform distribution of powder particles on the flat glass sample holder, thus resulting in the distortion of observed diffraction intensities from their ideal values. The introduction of a preferred orientation correction for the (0 -1 1) crystallographic plane finally led to a satisfying Rietveld fit. The Rietveld plots are shown in Figure S16-S20.
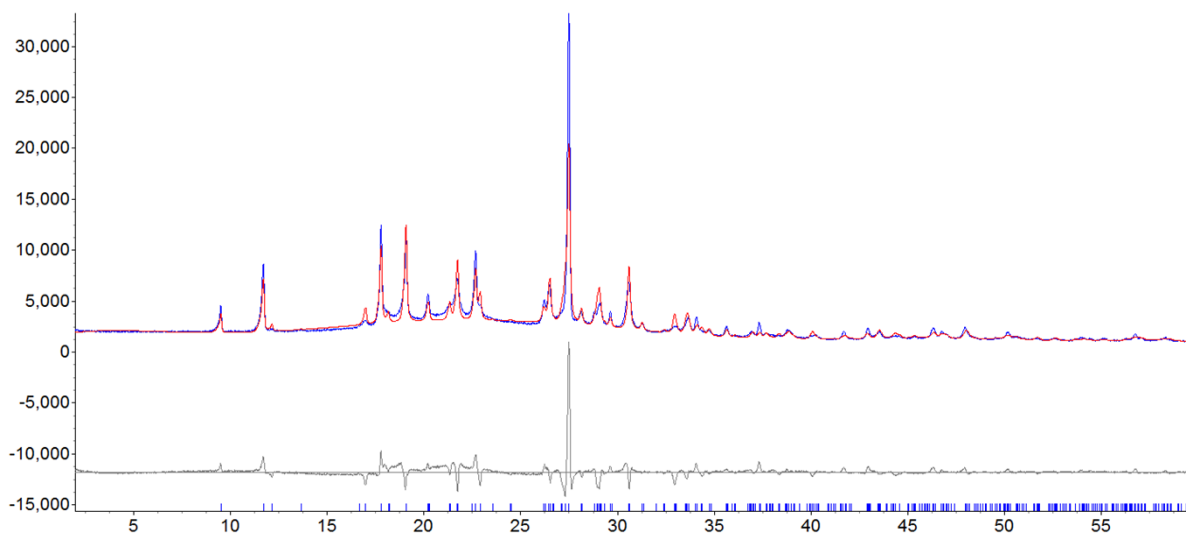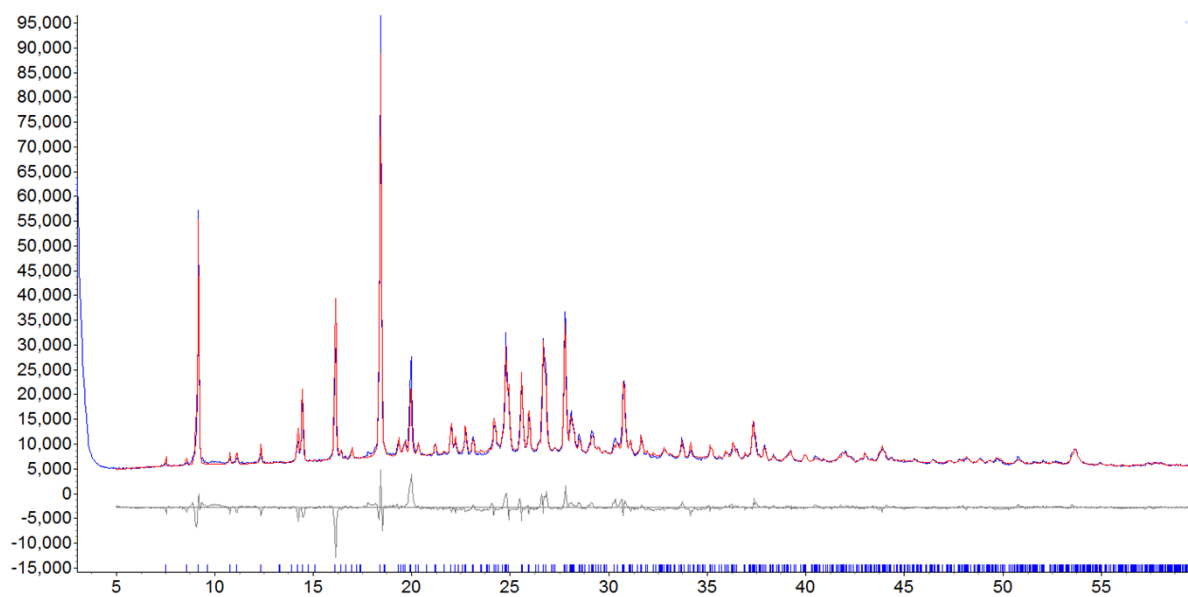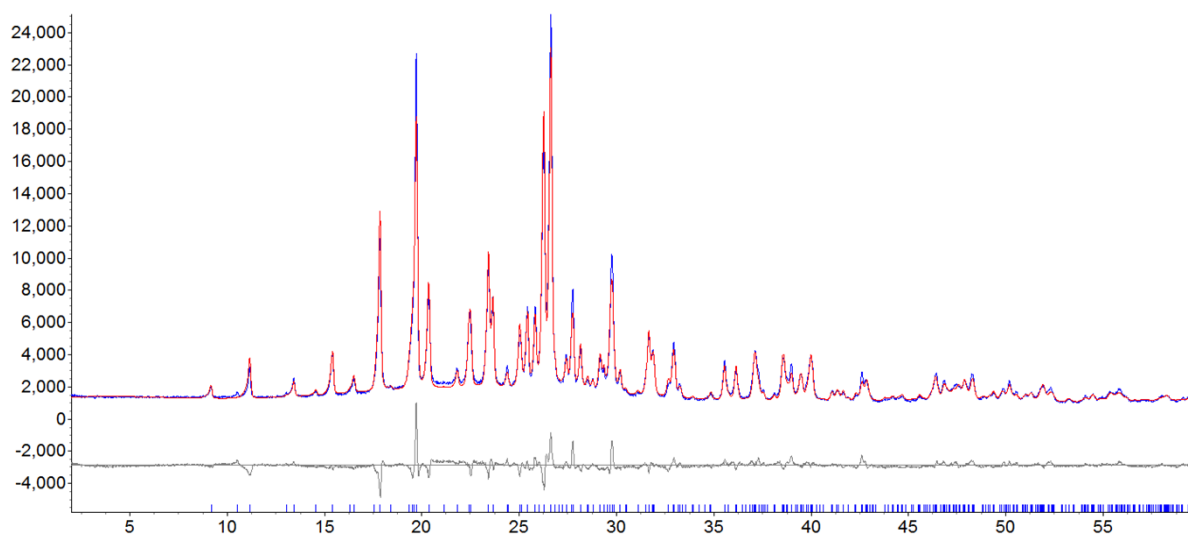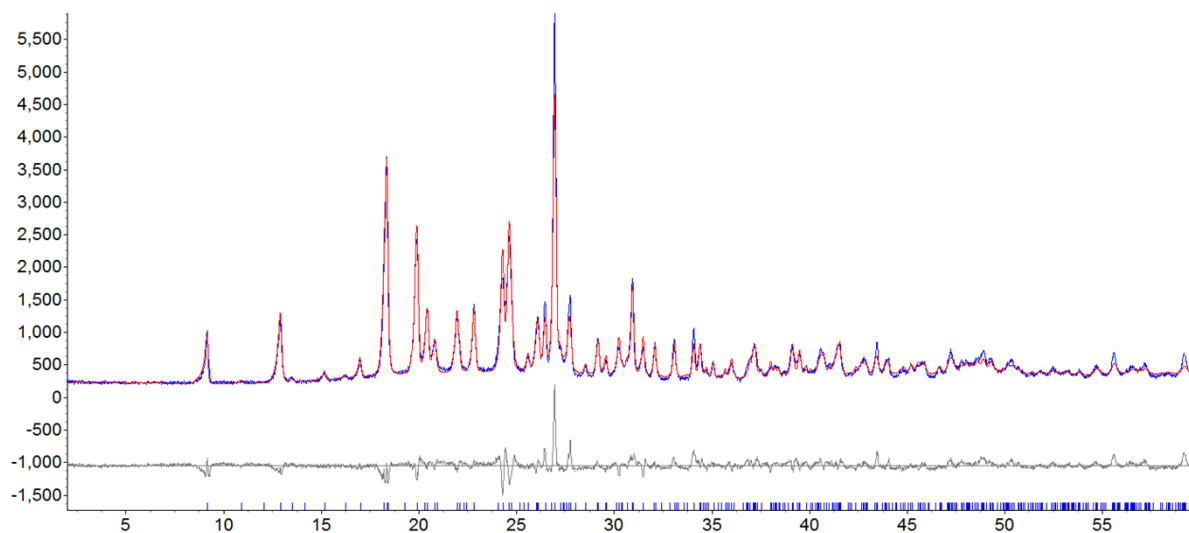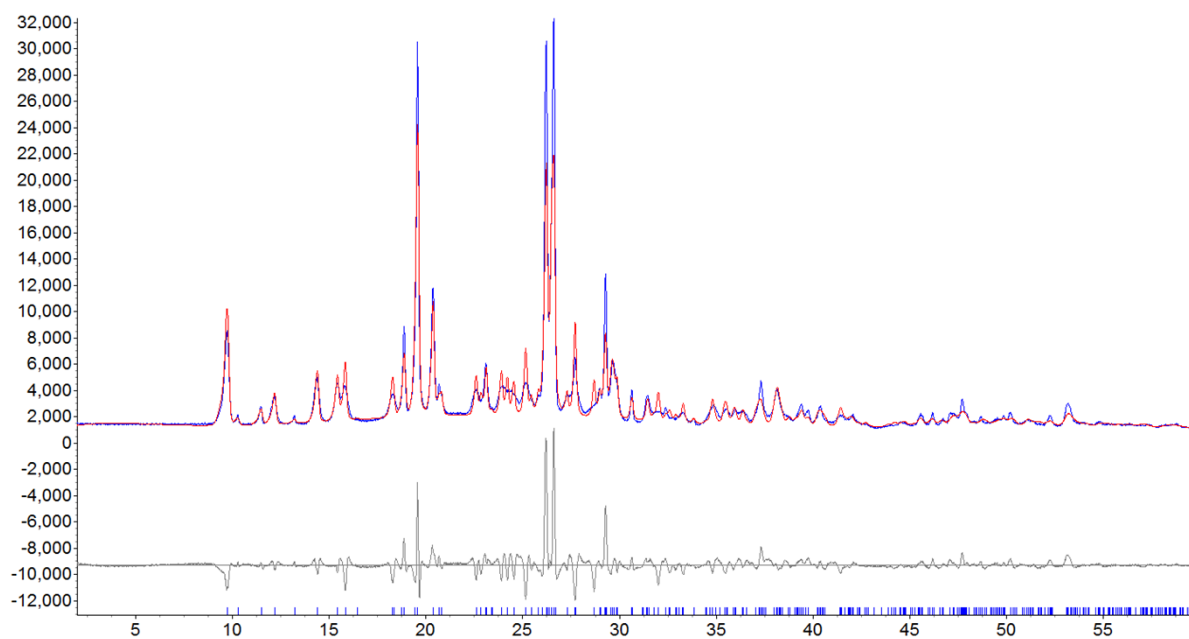

Figure S16. Rietveld plot for **9-F** (*red*: calculated, *blue*: measured, *grey*: difference). The peak positions are represented with tick marks (*x*-axis: 2θ values, *y*-axis: counts). $R_{wp} = 0.118$.

Figure S17. Rietveld plot for **9-Cl** (*red*: calculated, *blue*: measured, *grey*: difference). The peak positions are represented with tick marks (*x*-axis: 2θ values, *y*-axis: counts). $R_{wp} = 0.060$.

Figure S18. Rietveld plot for **9-Br** (*red*: calculated, *blue*: measured, *grey*: difference). The peak positions are represented with tick marks (*x*-axis: 2θ values, *y*-axis: counts). $R_{wp} = 0.067$.

16

Figure S19. Rietveld plot for **9-I** (*red*: calculated, *blue*: measured, *grey*: difference). The peak positions are represented with tick marks (*x*-axis: 2θ values, *y*-axis: counts). $R_{wp} = 0.096$.

Figure S20. Rietveld plot for **9-CH$_3$** (*red*: calculated, *blue*: measured, *grey*: difference). The peak positions are represented with tick marks (*x*-axis: 2θ values, *y*-axis: counts). $R_{wp} = 0.141$.

4.4. Qualitative powder X-ray diffraction (PXRD) studies of the 9-X salts
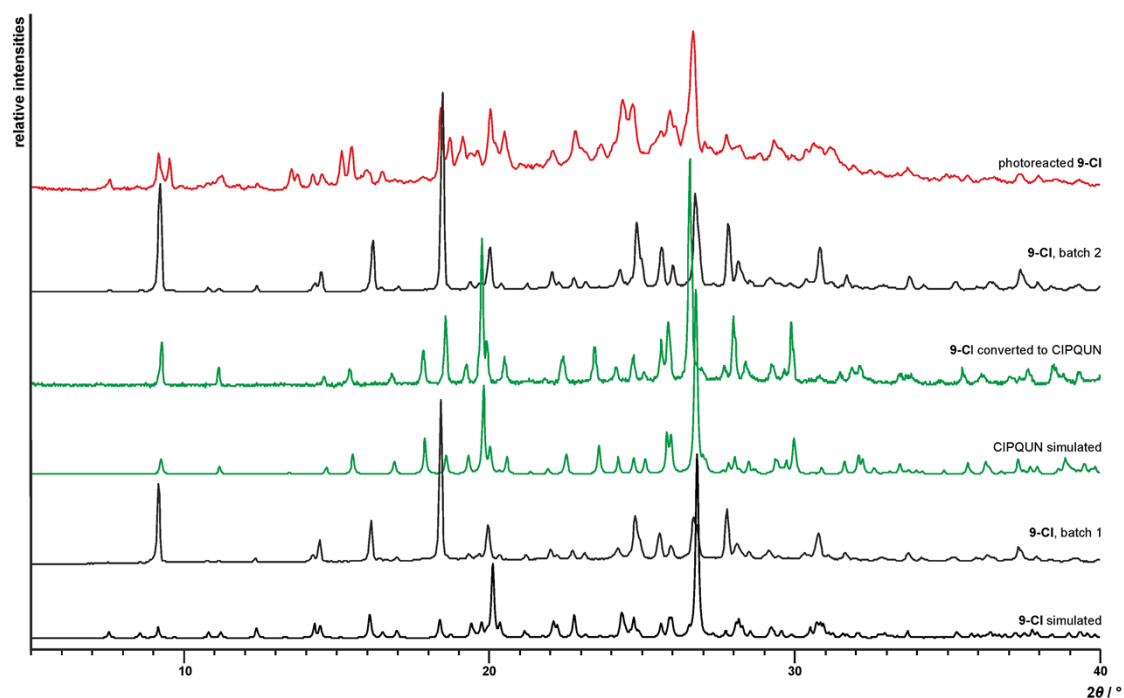
Figure S21. PXRD patterns of (from bottom to top): **9-Cl** (simulated), **9-Cl** (batch 1), CIPQUN (simulated), CIPQUN (from **9-Cl** upon spontaneous conversion), **9-Cl** (batch 2, from synthesis) and partially photoreacted **9-Cl** (batch 2). The powder pattern of the partially photoreacted batch of **9-Cl** (red) reveals diffraction peaks that correspond to **9-Cl**. This suggests that **9-Cl** is unlikely to convert into CIPQUN during UV irradiation.
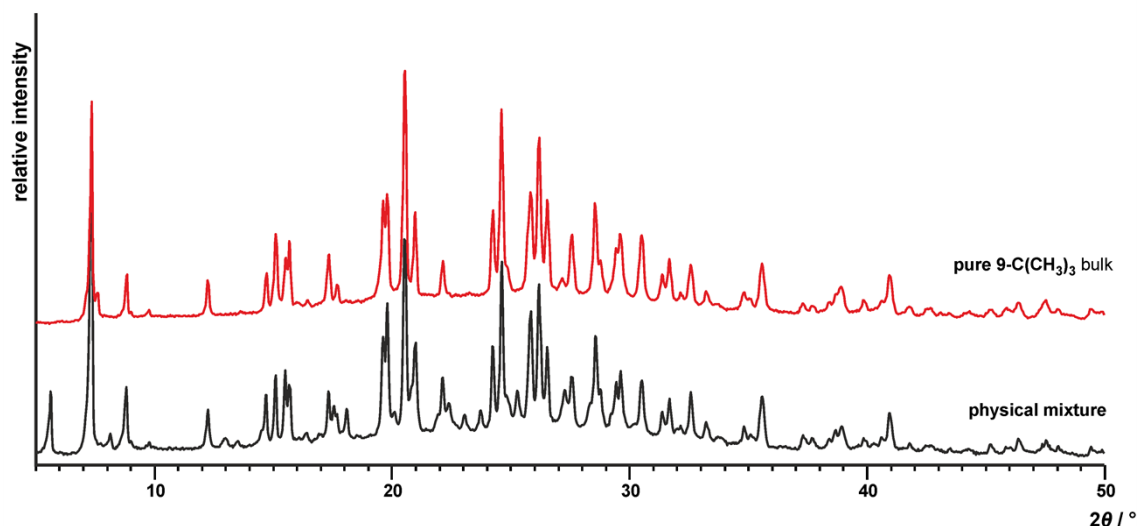
Figure S22. PXRD pattern of a physical mixture of 9-tert-butylacridizinium bromide forms (black) and pure **9-C(CH$_3$)$_3$** (red) obtained through thermal dehydration and rehydration. The Rietvels plot for **9-C(CH$_3$)$_3$** is shown in Figure S15.

5. Photoreactivity studies

The acridizinium salts **9-X** (~100 mg) were pressed onto watch glasses and placed directly in front of a *Saville Proslide Solo* slide projector (250 W, 12 V, 8000 lm lamp; fitted with a *Raynox* projection zoom lens 75-125 mm f3.5). The UV filter was removed during the photoreactivity studies. The samples were UV-irradiated for 5-24 hours. The ^{1}H NMR spectra of the photoreacted solids are shown in Figures S22-S27.

The assignment of the dominant regioisomers of the **9-Cl**, **9-Br** and **9-CH₃** photodimers was based on symmetry arguments and chemical shift differences in the ^{1}H NMR spectra. The assignment of the photoproducts as **ht** dimers was based on the chemical shifts of the protons H_6 and H_{11}: in case a **hh** isomer is formed, the bridgehead hydrogen atoms (*i.e.* H_6 and H_{11}) would show as singlets in the ^{1}H NMR spectrum, while a **ht** dimer would display doublets. Our ^{1}H NMR analyses revealed that the dominant photoproducts display two sets of doublets (J = 10.7-10.8 Hz). The *anti* nature of the isomers was determined by an analysis of the chemical shifts of the bridgehead protons (H_6 and H_{11}). In the *anti* isomer, the pyridinium ring interacts with the phenyl ring in a weak donor-acceptor fashion. This causes a slight decrease of the positive charge on the nitrogen atom and a concomitant shifting of the chemical shift of H_6 upfield relative to the peaks expected to be seen in the *syn* isomer.[15] The reverse applies for atom H_{11}. This transannular effect is particularly evident when the peaks referring to H_1 - H_4 (the pyridinium protons) are inspected. As the π-donor strength of the substituent on the opposite phenyl ring increases, the pyridinium protons are shifted to higher field.
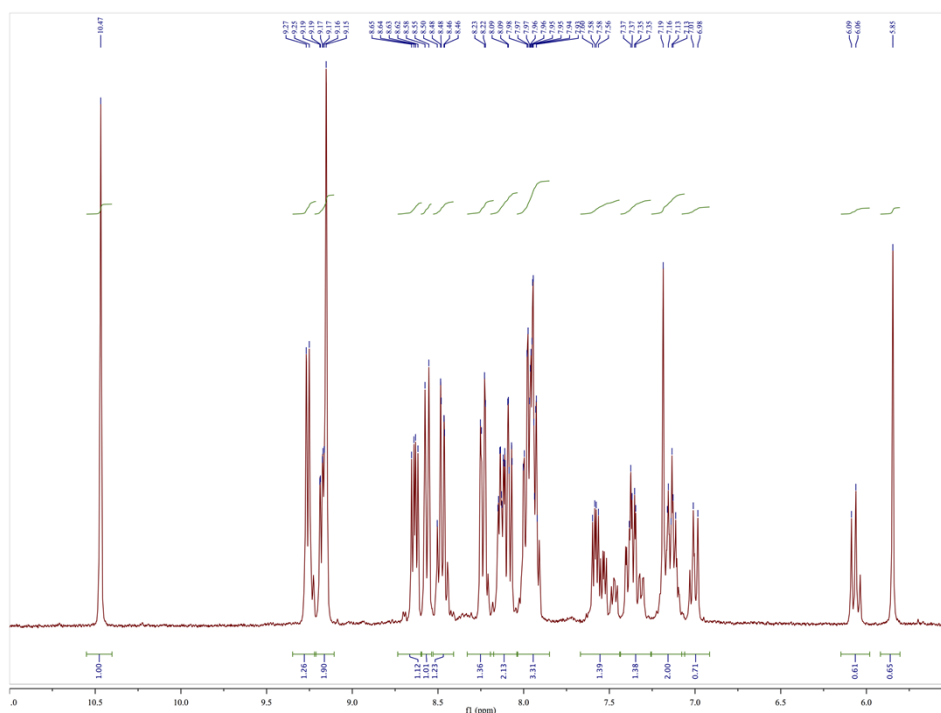

Figure S23. ^{1}H NMR spectrum of **9-F** after 24 hours of UV irradiation. The spectrum reveals the formation of multiple products in poor yields.
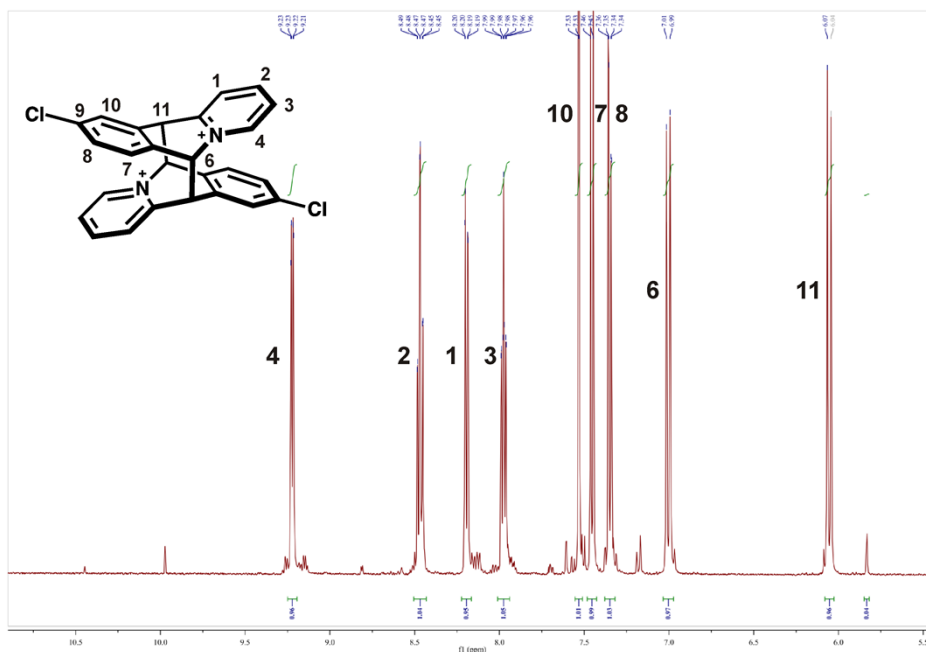
Figure S24. ¹H NMR spectrum of **9-Cl** after 5 hours of UV irradiation. The spectrum reveals the predominant formation of the *anti*-head-to-tail photodimer of **9-Cl**.
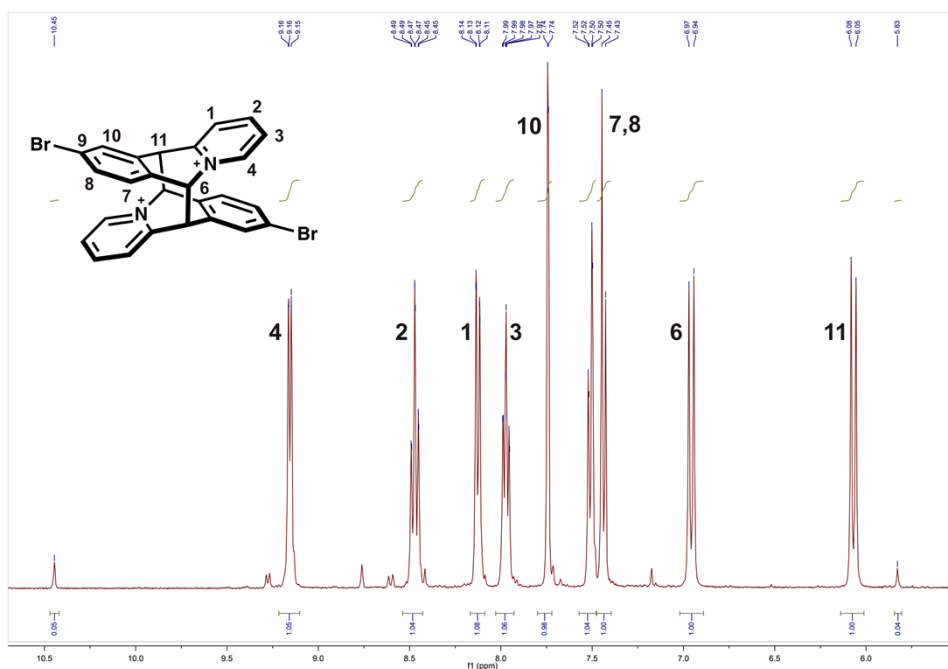

Figure S25. ¹H NMR spectrum of **9-Br** after 5 hours of UV irradiation. The spectrum reveals the predominant formation of the *anti*-head-to-tail photodimer of **9-Br**.
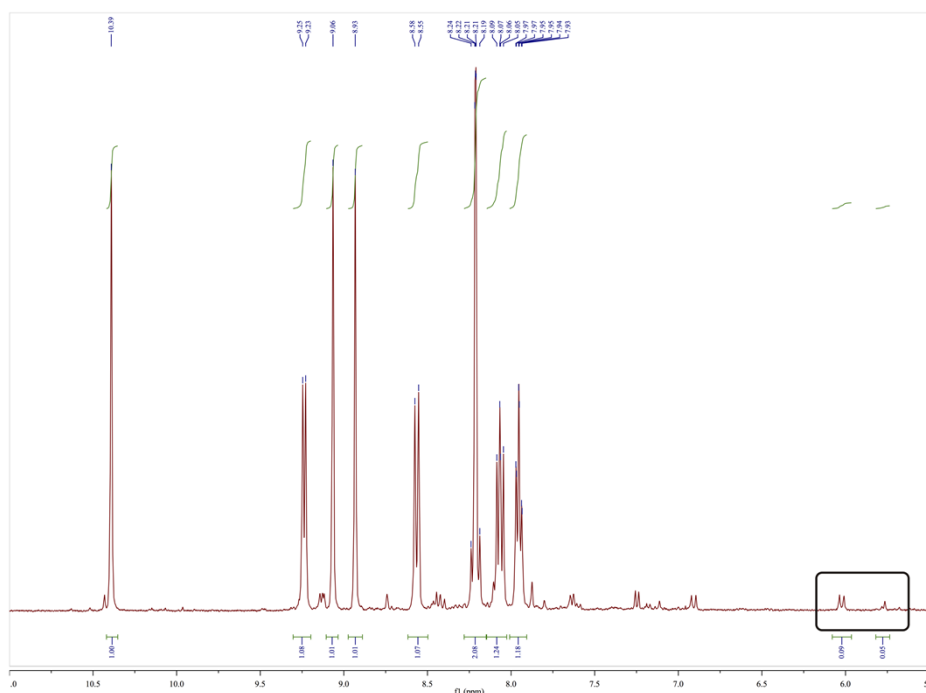
Figure S26. ^{1}H NMR spectrum of **9-I** after 24 hours of UV irradiation. The spectrum reveals that **9-I-Br** reacts non-regioselective in poor yields. The highlighted region of the spectrum indicates the formation of more than one isomer.
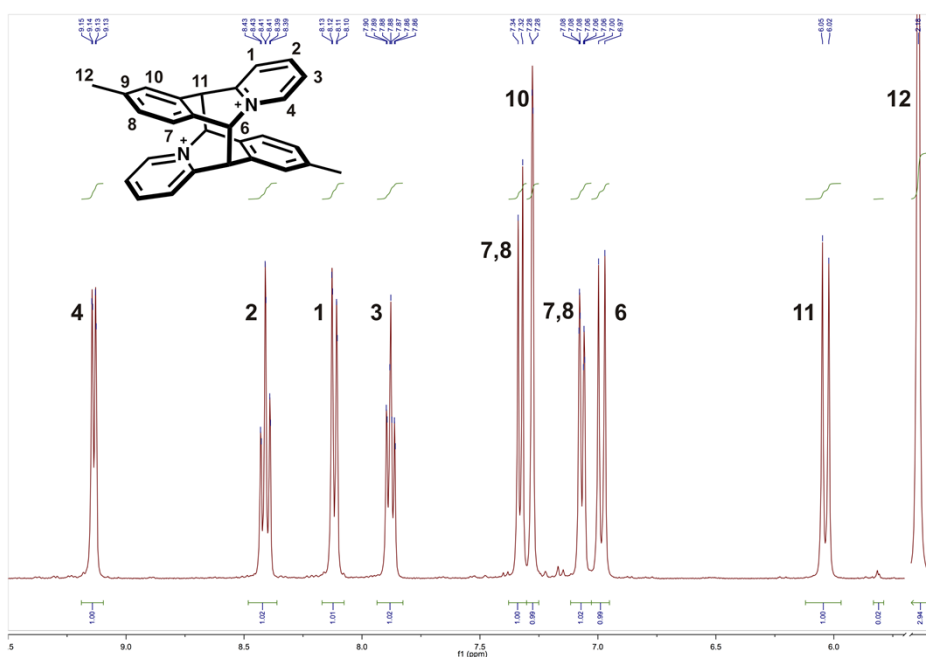

Figure S27. ^{1}H NMR spectrum of **9-CH₃** after 5 hours of UV irradiation. The spectrum reveals the predominant formation of the *anti*-head-to-tail photodimer of **9-CH₃**.
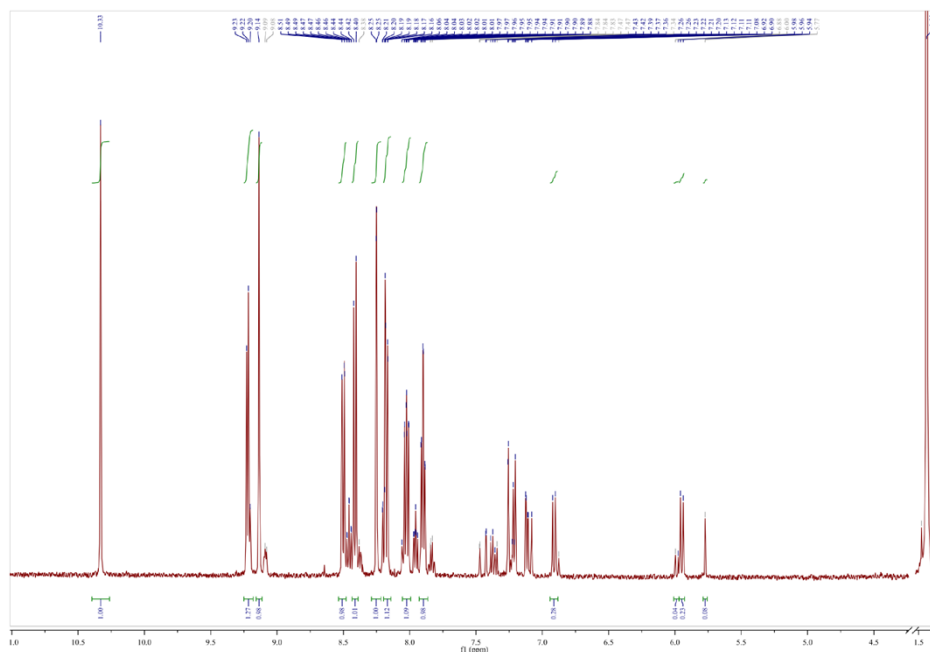
Figure S28. ^{1}H NMR spectrum of **9-C(CH$_3$)$_3$** after 5 hours of UV irradiation. The spectrum reveals that **9-C(CH$_3$)$_3$** reacts relatively non-regioselectively in poor yields.

A ^{1}H-^{1}H NMR NOESY experiment was performed on a sample of the photoproduct of **9-Br** to unambiguously demonstrate a correlation between H$_4$ and H$_{10}$ and, thus, confirm the formation of the *anti*-**ht** isomer (Fig. S28).
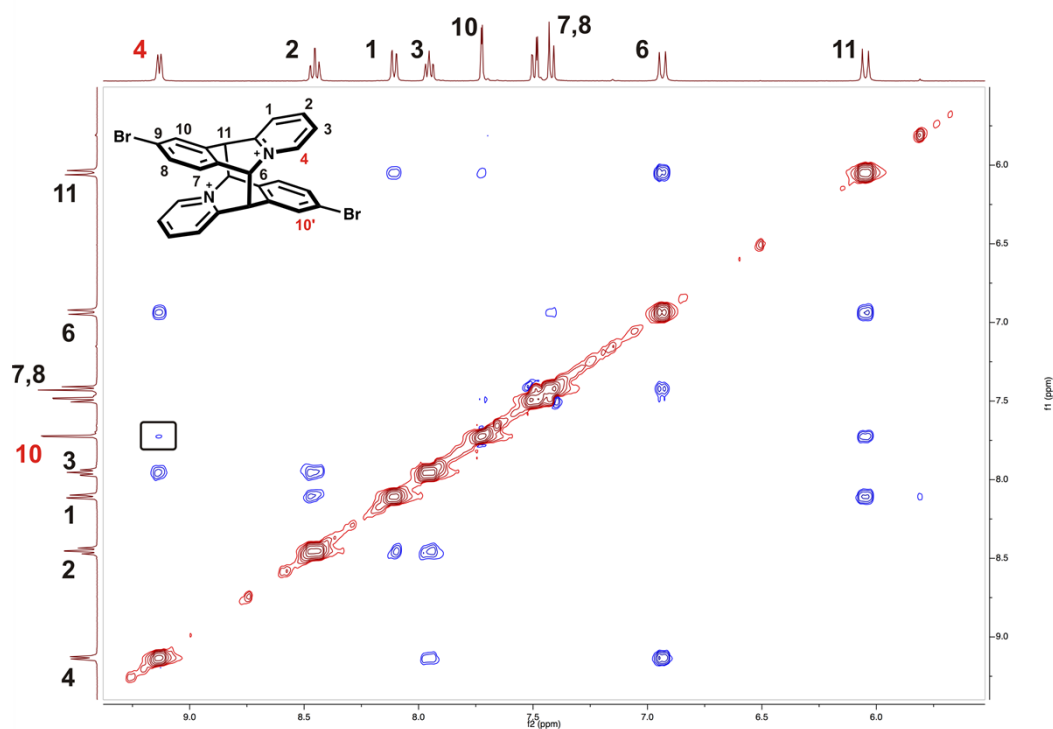

Figure S29. NOESY ^{1}H NMR spectrum of the photodimer of **9-Br** showing a through-space interaction between protons 4 and 10' (highlighted in the black square), thus confirming the *anti*-head-to-tail nature of the photoproduct.

To determine the relative reaction rates of the solids, separate samples were gently ground and placed in crystallisation dishes, and subsequently UV-irradiated utilising two single wavelength lamps (366 nm, 10 W) for 58 days at room temperature. The samples were investigated by ^{1}H NMR spectroscopy after 3, 6, 9, 12, 24, 30 and 60 days to monitor the progress of the [4+4] photodimerisation. The samples were mixed regularly to ensure even UV-irradiation of the samples. The progress of the photodimerisation over a course of 60 days is shown in Table S3 and Figures S29-S31.

Table S3. Progress of the photodimerisation of **9-Cl**, **9-Br** and **9-CH₃** over a course of 60 days (expressed in % yield).

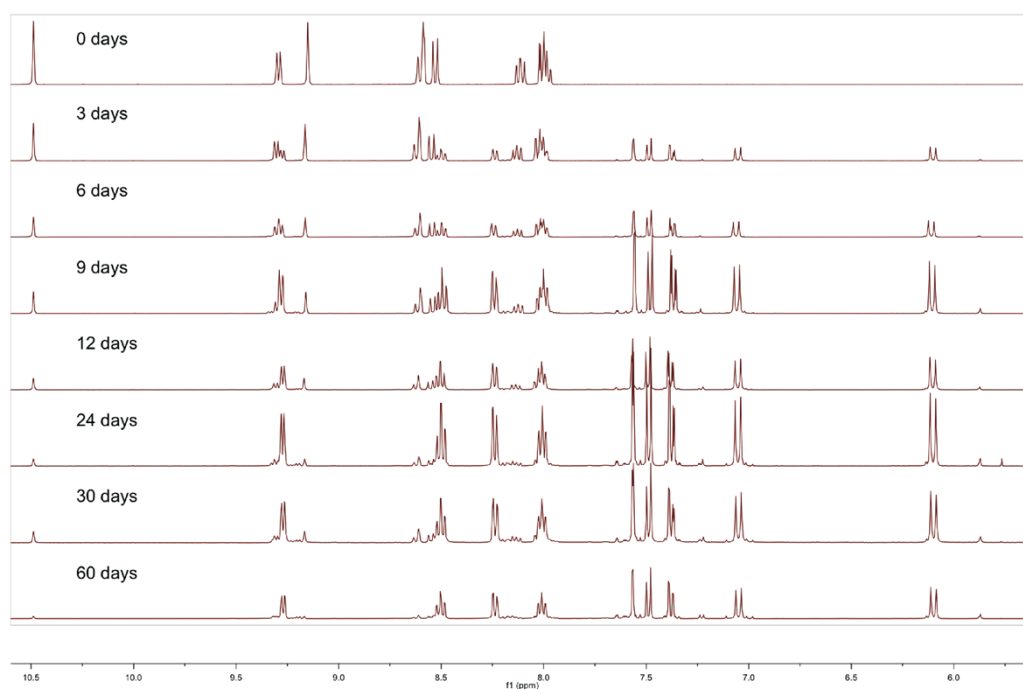| Time / days	0	3	6	9	12	24	30	60
9-Br	0	27.8	40.2	50.3	64.0	72.4	72.9	86.7
9-Cl	0	37.9	55.9	78.9	80.6	93.2	89.3	93.2
9-CH₃	0	24.6	36.7	30.9	34.6	51.8	45.6	66.5

Figure S30. The progress of the photodimerisation of **9-Cl** over a course of 60 days.
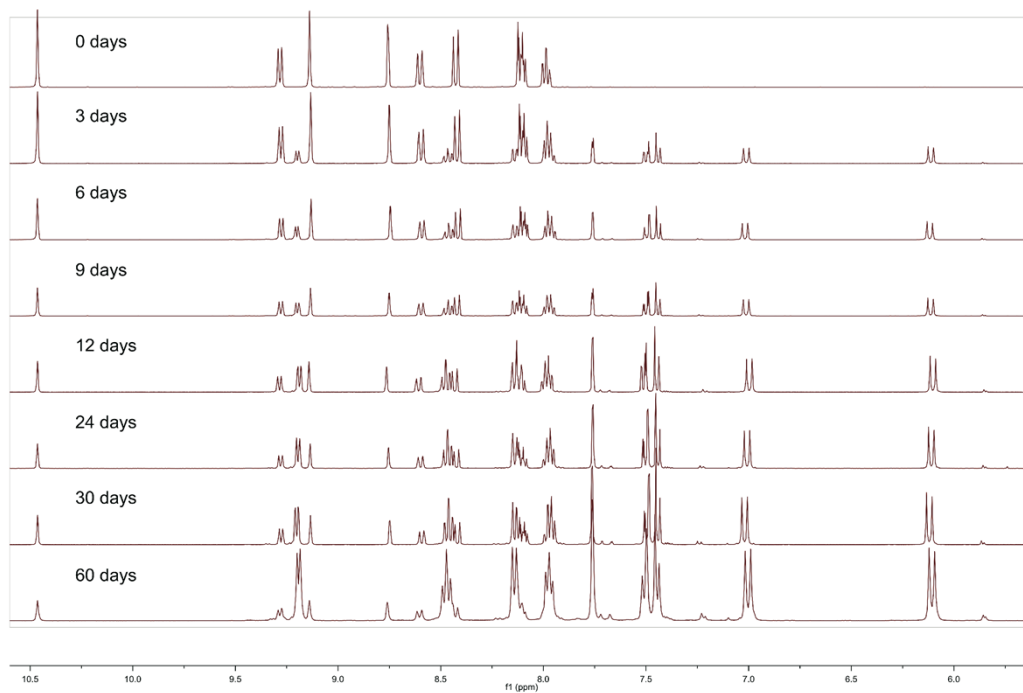
23

Figure S31. The progress of the photodimerisation of **9-Br** over a course of 60 days.
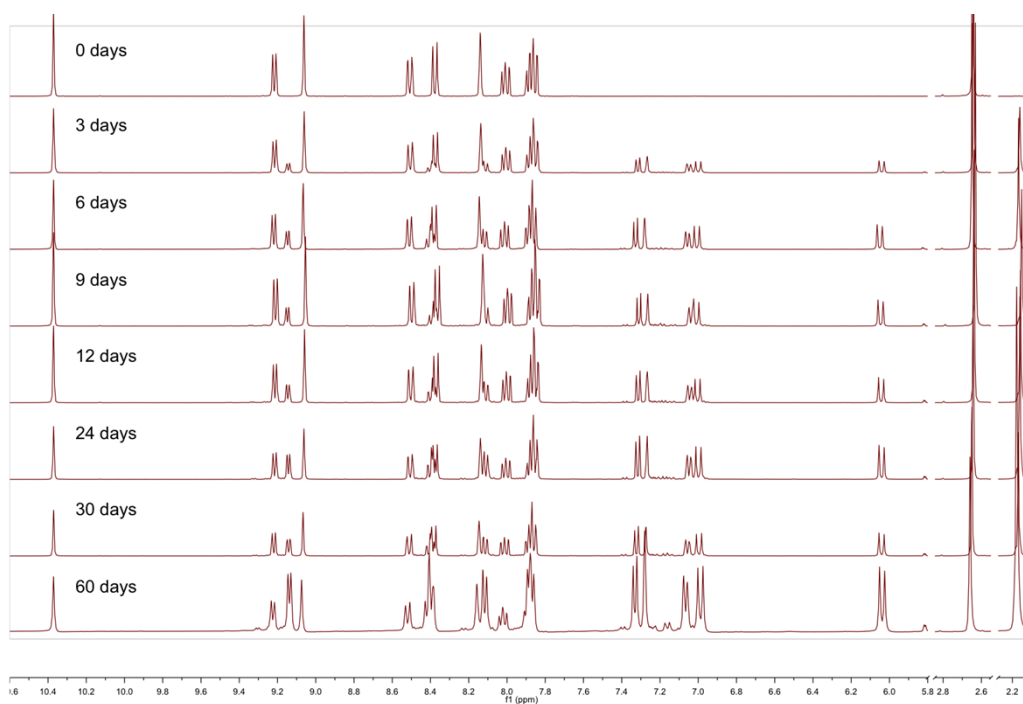

Figure S32. The progress of the photodimerisation of **9-CH₃** over a course of 60 days.

6. Analysis of frontier orbitals

Two pairs of 9-chloroacridizinium cations in the *anti*-**ht** and *syn*-**ht** orientations were extracted from the **9-Cl** crystal structure. Geometry optimisation of both moieties was performed in the program Gaussian03[16] at the DFT-B3LYP[17] level of theory with a 6-311G** basis set. During the optimisation, positions of the non-hydrogen atoms were constrained. Images of the frontier molecular orbitals were prepared in the program *Jmol*.[18]

7. Thermal analyses

Thermogravimetric analyses (TGA) were performed on a *Mettler Toledo TGA/SDTA851^e*. In a typical experiment, 10-15 mg of sample were placed in a 100 µL aluminium pan and heated in the 30-450 °C temperature range at 10 K min^{-1}. All samples were heated in a N_2 atmosphere (gas flow rate: 30 mL min^{-1}).

Differential-scanning calorimetry (DSC) experiments were performed on a *Mettler Toledo DSC822^e*. In a typical experiment, 2-4 mg of sample were placed in a 40 µL standard aluminium pan and heated in the 25-300 °C temperature range at 10 K min^{-1}. All samples were studied in a N_2 atmosphere (gas flow rate: 80 mL min^{-1}). The TGA and DSC thermograms were analysed using *STAR^e software v*.10.00. The thermograms of solids **9-X** are shown in Figures S32-S37.
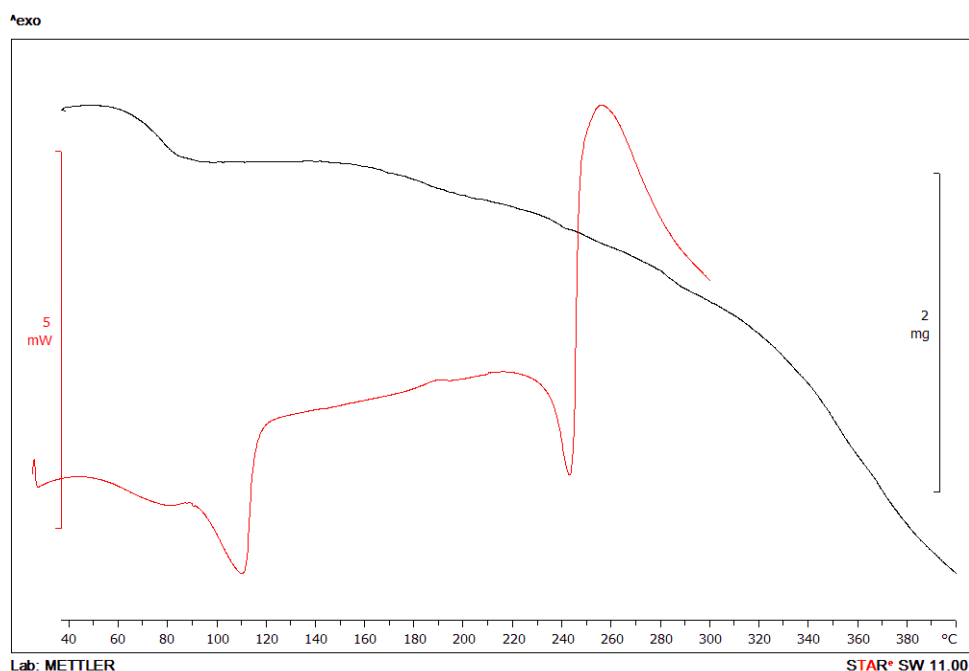

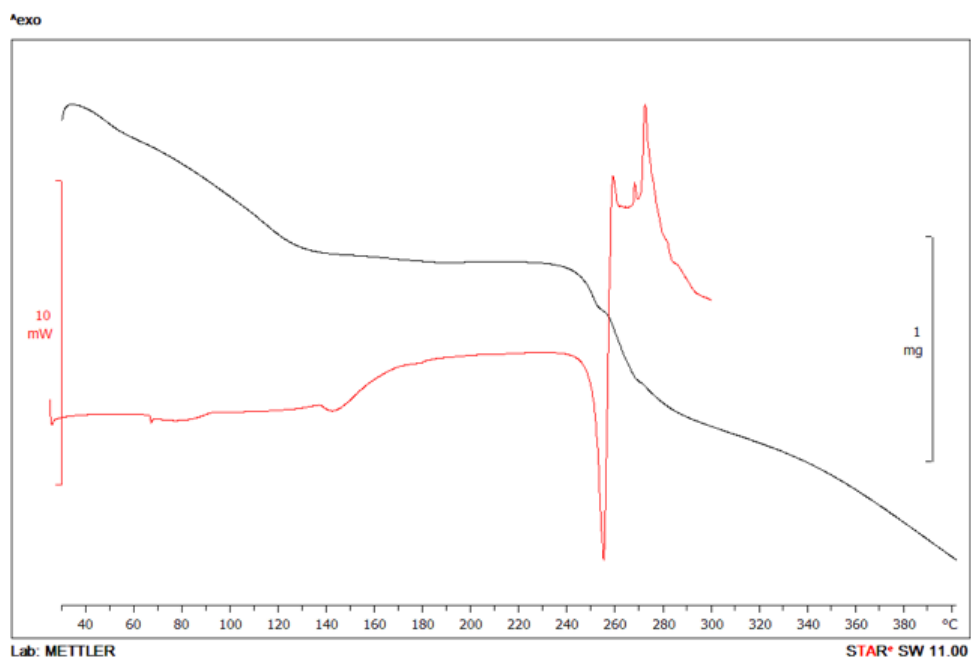**Figure S33.** DSC and TGA thermograms of **9-F** shown in red and black, respectively.

Figure S34. DSC and TGA thermograms of **9-Cl** shown in red and black, respectively.
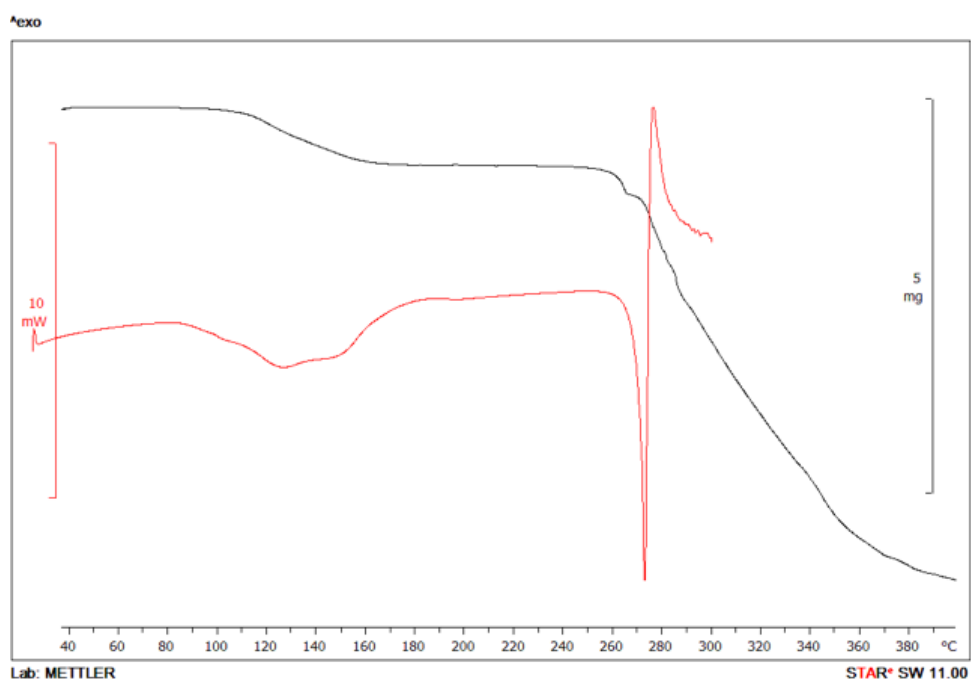

Figure S35. DSC and TGA thermograms of **9-Br** shown in red and black, respectively.
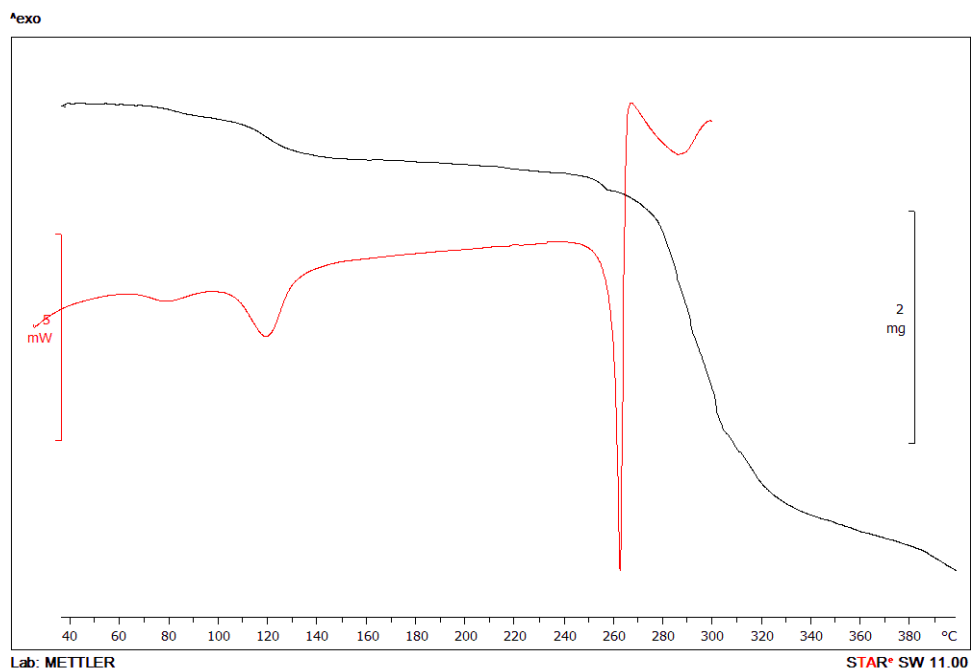
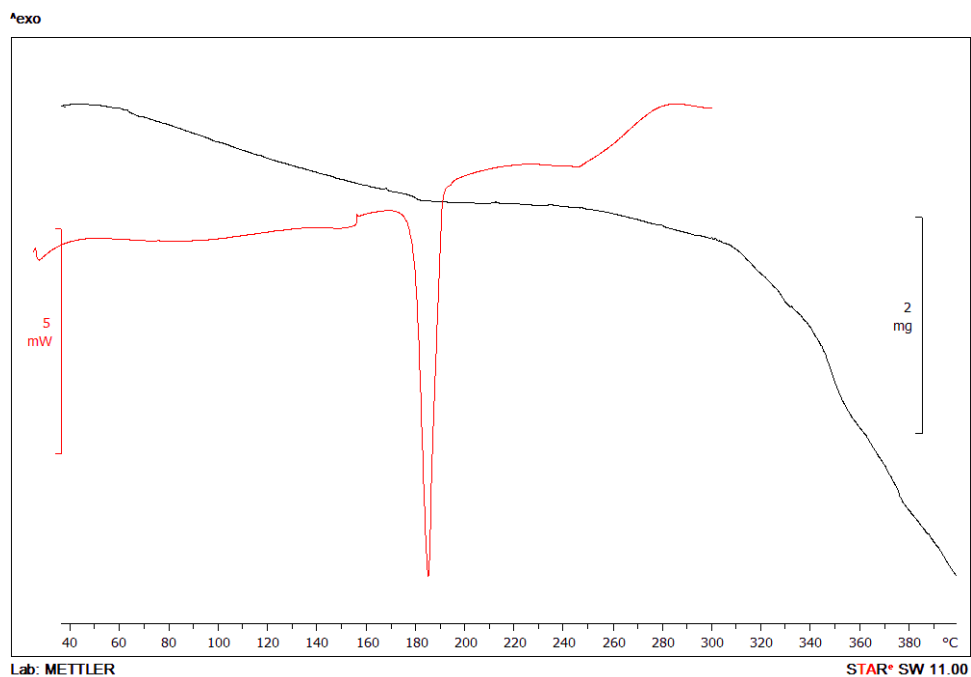**Figure S36.** DSC and TGA thermograms of **9-I-Br** shown in red and black, respectively.

Figure S37. DSC and TGA thermograms of **9-CH₃** shown in red and black, respectively.
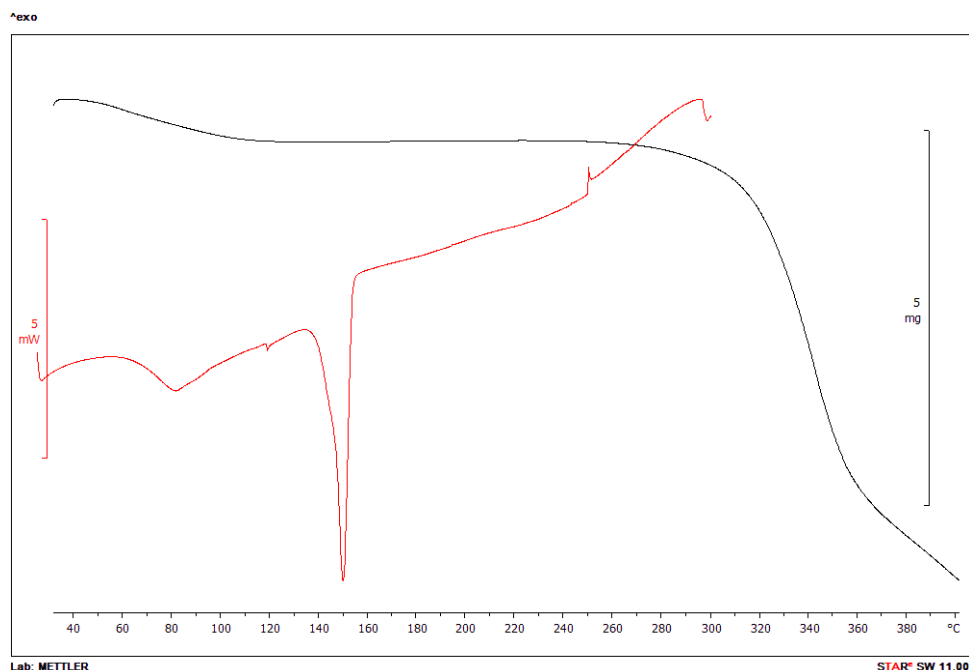
Figure S37. DSC and TGA thermograms of **9-C(CH₃)₃** shown in red and black, respectively.

8. References

1. S. T. Hobson, J. D. Boecker, J. H. Gifford, T. L. Nohe, and C. H. Wierks, *J. Heterocyclic Chemistry*, 2003, **40**, 277–282.
2. L. E. Bradsher, C. K. Beavers, *J. Am. Chem. Soc.*, 1955, **77**, 4812–4813.
3. C. K. Bradsher and J. C. Parham, *J. Org. Chem*, 1963, **28**, 83–85.
4. R. W. W. Hooft, *Collect*, 1998.
5. Z. Otwinowski and W. Minor, in *Methods in Enzymology, Macromolecular Crystallography Part A, edited by C. E. Carter Jr & R. M. Sweet*, New York: Academic Press, 1997, vol. 276, pp. 307–326.
6. G. M. Sheldrick, *Acta Crystallogr.* 2008, **A64**, 112–22.
7. Coelho, A.A., *TOPAS Academic. Version 4.1., Coelho Software*, Brisbane, Australia 2007.
8. A. Boultif and D. Louër, *J. Appl. Crystallogr.*, 2004, **37**, 724–731.
9. W. I. F. David, K. Shankland, J. van de Streek, E. Pidcock, W. D. S. Motherwell, and J. C. Cole, *J. Appl. Crystallogr.*, 2006, **39**, 910–915.
10. H. M. Rietveld, *J. Appl. Crystallogr.*, 1969, **2**, 65–71.
11. S. J. Clark, M. D. Segall, C. J. Pickard, P. J. Hasnip, M. I. J. Probert, K. Refson, and M. C. Payne, *Z. Kristallogr.*, 2005, **220**, 567–570.
12. J. Perdew, K. Burke, and M. Ernzerhof, *Phys. Rev. Lett.*, 1996, **77**, 3865–3868.
13. S. Ehrlich, J. Moellmann, W. Reckien, T. Bredow, and S. Grimme, *ChemPhysChem*, 2011, **12**, 3414–20.
14. A. Rappe, K. Rabe, E. Kaxiras, and J. Joannopoulos, *Phys. Rev. B*, 1990, **41**, 1227–1230.
15. H. Ihmels, D. Leusser, M. Pfeiffer, and D. Stalke, *J. Org. Chem.*, 1999, **64**, 5715–5718.
16. M. J. Frisch, G. W. Trucks, H. B. Schlegel, G. E. Scuseria, M. A. Robb, J. R. Cheeseman, J. A. Montgomery, Jr., T. Vreven, K. N. Kudin, J. C. Burant, J. M. Millam, S. S. Iyengar, J. Tomasi, V. Barone, B. Mennucci, M. Cossi, G. Scalmani, N. Rega, G. A. Petersson, H. Nakatsuji, M. Hada, M. Ehara, K. Toyota, R. Fukuda, J. Hasegawa, M. Ishida, T. Nakajima, Y. Honda, O. Kitao, H.

Nakai, M. Klene, X. Li, J. E. Knox, H. P. Hratchian, J. B. Cross, V. Bakken, C. Adamo, J. Jaramillo, R. Gomperts, R. E. Stratmann, O. Yazyev, A. J. Austin, R. Cammi, C. Pomelli, J. W. Ochterski, P. Y. Ayala, K. Morokuma, G. A. Voth, P. Salvador, J. J. Dannenberg, V. G. Zakrzewski, S. Dapprich, A. D. Daniels, M. C. Strain, O. Farkas, D. K. Malick, A. D. Rabuck, K. Raghavachari, J. B. Foresman, J. V. Ortiz, Q. Cui, A. G. Baboul, S. Clifford, J. Cioslowski, B. B. Stefanov, G. Liu, A. Liashenko, P. Piskorz, I. Komaromi, R. L. Martin, D. J. Fox, T. Keith, M. A. Al-Laham, C. Y. Peng, A. Nanayakkara, M. Challacombe, P. M. W. Gill, B. Johnson, W. Chen, M. W. Wong, C. Gonzalez, and J. A. Pople, *Gaussian 03, Revision C.02, Gaussian, Inc.*, Wallingford CT, 2004.

17. P.J. Stephens, F.J. Devlin, C.F. Chabalowski and M.J. Frisch, *J.Phys.Chem.*, 1994, **98**, 11623-11627.

18. Jmol: an open-source Java viewer for chemical structures in 3D. http://www.jmol.org/